A pocket-integrated miniature, dual-band, and high gain textile MIMO antenna for 5G and WiFi wearable applications

scientific reports

Check for updates

OPEN

A pocket-integrated miniature, dual-band, and high gain textile MIMO antenna for 5G and WiFi wearable applications

Deepti Sharma[1], Rakesh N. Tiwari[2], Dinesh Kumar Singh[1] & Ladislau Matekovits[3,4,5]✉

This paper reports a miniature low-profile denim textile 2-port MIMO (multiple-input-multiple-output) antenna for dual-bands: 5G sub-6 3.5 GHz and Wi-Fi 5.2 GHz wearable applications. This MIMO antenna has impedance bandwidths and peak gain of 310 MHz and 8.3 dBi and 950 MHz 13.0 dBi at 3.5 and 5.2 GHz, respectively. This MIMO antenna has a compact area of 0.078 λ_0^2, with both antenna elements of the MIMO being a modified elliptical patch, L-shaped stubs for impedance matching, and a circular decoupling ring to achieve > 25 dB port isolation. The designed antenna is very tiny and integrated into the shirt's pocket. It is tested in two positions, i.e., hidden (integrated inside the pocket, for example, military applications) and visible (when integrated on the pocket surface for conventional communication). Moreover, the antenna's working is analyzed in these positions (hidden and visible), and it was found that it functions well in both 5G sub-6 GHz and Wi-Fi frequency bands with nearly close gain values and communication range. This MIMO antenna has a very small ECC (envelope correlation coefficient) of 0.006/0.002 in both frequency bands, which shows high channel isolation. The 1 gm/10 gm SAR (specific absorption rate) values at 3.5 and 5.2 GHz are 0.034/0.057 and 0.026/0.0132 W/Kg, respectively, substantially lesser than the recommended values of FCC/ICNIRP.

Wearable textile antennas are attracting many researchers due to their popularity in numerous areas, such as healthcare, military, sports, space, etc. These antennas can be fabricated on some popular materials: denim, felt, silk, cotton, etc., and play a crucial role in communicating with external or implantable devices to exchange health-related data wirelessly[1]. In the upcoming time, with the growth of 5G and 6G networks, the entire nature of communication will be based on MIMO antennas because MIMO antenna can provide reliable communication due to their low path losses, high channel capacities, high data rate, and increased communication range without extra input power requirements compared to the single-port antenna[2–4]. The wearable devices operate close to the human body, and the human body behaves as a lossy channel owing to the high dielectric properties of different tissue layers, which may lead to low data rate/limited communication distance. Due to this, the MIMO antenna is a superior contender to the conventional single-port antenna in the lossy and challenging human-body environment.

Recently, many single-port and MIMO antennas were recommended for wearable textile applications. A single-band textile MIMO antenna was given in[5]. This antenna operates in the ISM (Industrial Scientific Medical) 2.45 GHz band but has poor port isolation (12 dB) of 1.67 dBi. Another wearable MIMO antenna with multiband operation, large footprints and high port isolation between the antenna elements was proposed in[6]. This antenna shows moderate gain at the operating frequency bands. An ultrawideband wearable antenna with a decent gain of 7.2 dBi was proposed for wearable applications, but this antenna has limited port isolation between the antenna elements and has relatively large footprints[7]. A wearable MIMO spiral button-form antenna with dual-band operation was proposed[8].

This antenna had decent isolation, gain, and bandwidth, but its structure had shorting pins that might have made it a bit unstable. Recently, two more wearable antennas with large footprints and optimum isolations

[1]Department of Electronics and Communication Engineering, G.L. Bajaj Institute of Technology and Management, Greater Noida, Lucknow, Uttar Pradesh 201306, India. [2]Department of Electronics and Communication Engineering, Madanapalle Institute of Technology and Science, Madanapalle, Andhra Pradesh 517325, India. [3]Department of Electronics and Telecommunications, Politecnico di Torino, 10129 Turin, Italy. [4]Faculty of Electronics and Telecommunications, Politehnica University Timişoara, 300006 Timişoara, Romania. [5]National Research Council of Italy, Istituto di Elettronica e di Ingegneria dell'Informazione e delle Telecomunicazioni, 10129 Turin, Italy. ✉email: ladislau.matekovits@polito.it

and gains were proposed[9,11]. A single-band wearable antenna was proposed for 2.4 GHz WBAN applications[10]. This semi-flexible antenna had a limited bandwidth (3.8%) and a moderate gain (3.81 dBi). Also, there was no consideration of bending, and SAR was not analyzed. A dual-band wearable antenna for sub-6 GHz wearable applications was designed[12]. It had good gain and broadband behaviour. Still, port isolation between antennas was insufficient (only 12 dB), which might lead to unfavourable interference between the ports. A quad-element MIMO antenna for wearable applications was proposed for 3.5 GHz frequency applications, with good isolation and bandwidth but with large antenna size[13]. Recent literature shows many wearable antennas[15–19] with multiband behaviour, wide bandwidth, and high gain for wearable multiband applications. However, these antennas are conventional single-port antennas and will provide limited data rates and low losses compared to the MIMO antennas.

This paper proposes a denim-based textile two-port MIMO antenna, tiny footprints of 24 mm × 24 mm and dual-band behaviour for 5G sub-6 GHz (3.5 GHz) and Wi-Fi 5.2 GHz resonating frequencies. The 3.5 GHz can support communication on the 5G platform, and the 5.2 GHz frequency band can support high data speeds, which will help transmit high-quality patient images to distant healthcare professionals. This MIMO antenna has a novel modified semi-elliptical patch antenna with microstrip feed, L-shaped stub, and circular decoupling ring to achieve high isolation between the antenna elements. The ground plane of the designed MIMO antenna has continuous slots that help to achieve high gain at both working frequency bands. Compared to the other reported antennas, as specified in Table 1, this antenna has the most compact size, low profile, sufficient bandwidth, high gain, and low SAR values. This antenna can fit inside the pocket, be hidden, or be integrated outside the shirt's pocket, as illustrated in (Fig. 1). Its behaviour in both positions is analysed and found satisfactory, covering the desired operating frequency bands of 3.5 and 5.2 GHz wearable applications. Also, the dual-band operation of this antenna makes it fit for wireless data/power telemetry, which is the common requirement of modern-day BAN (body area network) wearable devices[20]. The novelty of the proposed wearable textile antenna, as compared to the recently reported wearable antennas, can be summarized in the following points:

- The proposed antenna has the most compact size and low profile, which makes it easily integrated inside/outside the shirt's pocket and can support hidden/visible communications.
- This antenna has sufficient bandwidth and comparatively high gain.
- Due to dual-band operation of sub-6 3.5 GHz and WiFi 5.2 GHz, it can operate in a 5G environment and support high data rates, respectively.
- Low SAR values offered by this antenna make it safe for wearable applications.

Methodology

Antenna design

A dual-band MIMO antenna proposed in this paper is constructed on the 1 mm thick denim fabric substrate. The dielectric constant (ε_r) and the loss tangent (δ) are 1.72 and 0.04, respectively. An RF impedance/material analyzer (Agilent E4991A) was used to evaluate the dielectric constant, and a digital vernier gauge was used for the fabric's thickness measurement. A copper conducting material was used to construct conducting patterns of the textile antenna[21]. This 2-port textile MIMO antenna was designed in a 3D EM simulation tool, Ansys HFSS. Its layout is illustrated in (Fig. 2a,b), and its entire size is 24 mm × 24 mm. The design parameter values are mentioned in (Table 2).

Moreover, the MIMO antenna is intended for wearable textile applications. So, it is created on a multi-layer (skin-fat-muscle) chest phantom, as given in (Fig. 3). The permittivity and conductivity of skin, fat and muscle are considered from[22]. The proposed 2-port MIMO antenna elements are designed using a modified semi-elliptical geometry with microstrip feed. Each antenna has L-shaped stubs connected to the microstrip feeds for the desired matching, and a circular ring between the two modified elliptical radiating patches enhances port isolation. The ground plane of this antenna is slotted and helps to achieve high gain[23]. Finally, this MIMO

[Ref.] (Year)	[7] (2022)	[8] (2023)	[9] (2023)	[10] (2023)	[11] (2024)	[12] (2024)	[13] (2024)	Prop.
Antenna type	MIMO	MIMO	MIMO	Single	MIMO	MIMO	MIMO	MIMO
Isolation	15	20	19.8	–	20	12	20	25
Area (mm^2)	92 × 92	33 × 22.5	80 × 40	55 × 55	56 × 41	40 × 50	44 × 44	24 × 24
Area (λ_0^2)	0.75 × 0.75 (0.56)	0.38 × 0.26 (0.10)	1.67 × 0.81 (1.357)	0.37 × 0.25 (0.09)	0.41 × 0.3 (0.123)	0.47 × 0.40 (0.192)	0.63 × 0.63 (0.39)	0.28 × 0.28 (0.078)
Frequency (GHz)	2–14	3.4/5.3	5.6	2.4	4.0/8.1	4.6	4.3	3.5/5.2
Bandwidth (%)	120	11/08	34.87	3.8	110.5	74	2.2	11.4/17.5
Peak gain (dBi)	7.2	7.2/5.6	7.95	3.86	4.3	6.7	3.0	8.3/13.0
Bending analysis done	Yes	Yes	No	No	Yes	Yes	Yes	Yes
ECC	0.04	0.05	0.35	–	0.002	0.0005	0.015	0.006/0.002
SAR (W/Kg) 1 g/10 g	0.0125/– (at 50 mW)	0.36/0.35 0.51/0.53 (at 1 W)	–	–	100.6/66.7 39.6/25.2 (at 1 W)	1.93/– (at 1 W)	–	0.034/0.057 0.026/0.013 (at 0.5 W)

Table 1. Proposed antenna vs other wearable antennas.

Fig. 1. Schematic view of proposed textile MIMO antenna integrated inside the pocket for wearable communication (human body figure is adapted from[14]).

antenna operates at 3.5 and 5.2 GHz frequency bands with >25 dB port isolation and high gain: 8.3 and 13.0 dBi, respectively.

Technical route of wearable MIMO antenna design

The complete technical route, which explains the proposed wearable MIMO antenna design, is discussed below:

Literature study

This is the proposed work's first and most crucial part, as shown in (Fig. 4). Initially, the recent wearable MIMO antennas were studied[5–8,12,13]. Some of these MIMO antennas had certain limitations, such as optimum gain and dual-band behaviour, but large footprints[6,13]. Others had compact sizes, poor port isolation between antenna elements, and limited gain[5,12]. Some recently proposed antennas were single-port and might not compete with 5G/6G and future technologies that need MIMO antennas to support high data-rate communication. To address these issues in one antenna, it was necessary to design an ultra-compact MIMO antenna with highly isolated ports, high gain, flexible, and low SAR parameters.

Selection of antenna geometry

A simple low-profile microstrip patch antenna on the denim fabric substrate was considered. Denim fabric offers wearer comfort and flexibility, and the microstrip antenna is easy to design and fabricate. However, we have selected a semi-elliptical microstrip patch antenna. This geometry, as compared to rectangular and circular geometry, provided better miniaturization and isolation between the antenna elements when designed in the same area of 24 mm × 24 mm. We have not mentioned these results for brevity.

In the literature, many researchers have used elliptical geometry to design antennas for different objectives/applications. A two-port MIMO antenna was designed for 3.5 GHz wireless applications[24]. A half-elliptical

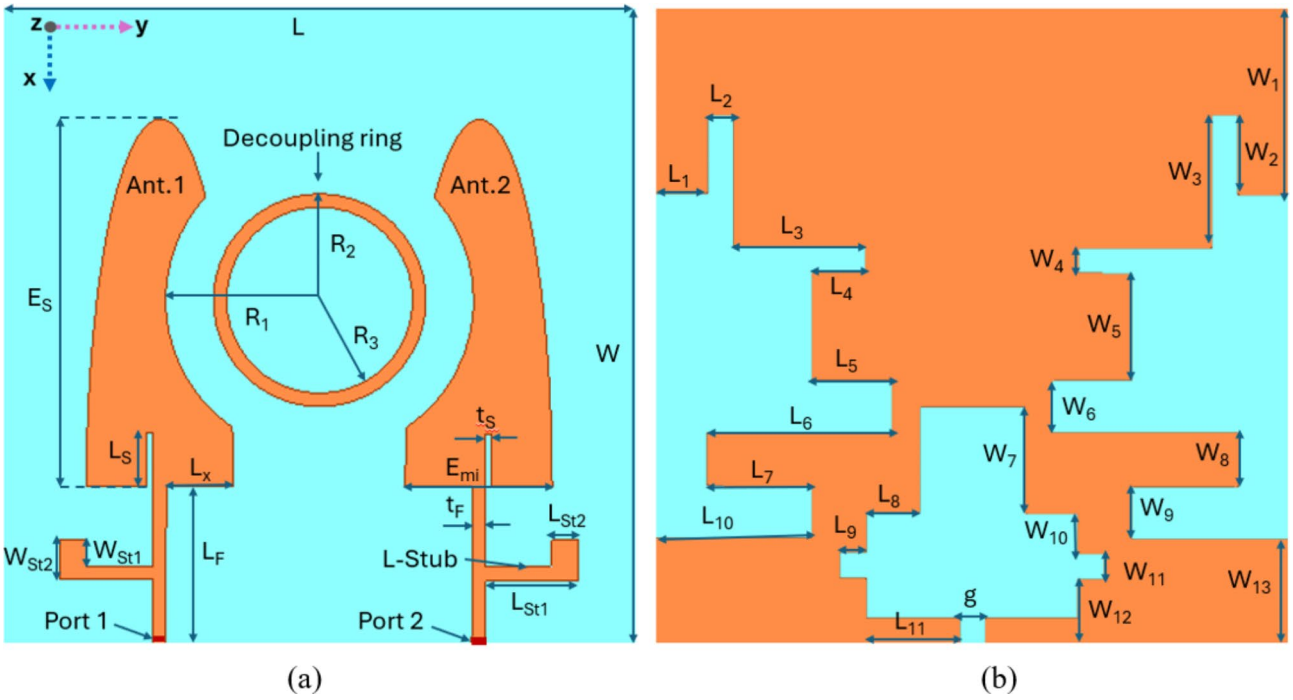

Fig. 2. Proposed wearable MIMO antenna: (**a**) Top radiating patch, (**b**) ground plane.

Parameter	Value (mm)	Parameter	Value (mm)	Parameter	Value (mm)	Parameter	Value (mm)
L	24	R_1	5.8	L_7	4.0	W_7	4.0
W	24	R_2	4.0	L_8	2.0	W_8	2.0
E_S	13.8	R_3	3.5	L_9	1.0	W_9	1.5
E_{mi}	5.5	t_S	0.25	L_{10}	6.0	W_{10}	2.0
L_S	2.0	t_F	0.5	L_{11}	3.5	W_{11}	1.0
L_x	2.2	L_1	2.0	W_1	7.0	W_{12}	2.5
L_F	6.0	L_2	1.0	W_2	3.0	W_{13}	4.0
L_{St1}	3.5	L_3	5.0	W_3	5.0	g	1.0
L_{St2}	1.0	L_4	2.0	W_4	1.0		
W_{St1}	1.0	L_5	3.0	W_5	4.0		
W_{St2}	1.5	L_6	7.0	W_6	2.0		

Table 2. Parameters of the proposed two-port wearable MIMO antenna.

patch antenna with super-wideband behaviour was proposed in[25]. A shorted elliptical patch antenna for GPS applications was proposed in[26]. In one research, an elliptical card patch antenna for UWB applications was proposed in[27], and a wideband elliptical patch antenna was proposed in[28]. However, in our proposed work, elliptical geometry assisted in miniaturization and port isolation between antenna elements of the proposed two-port antenna. The semi-elliptical antenna element used to design the proposed two-port MIMO antenna is significantly modified with a circular decoupling ring to provide more isolation between MIMO antenna elements, making this design novel.

MIMO antenna design on the chest phantom

From the very first step, the MIMO antenna was designed on the canonical phantom (skin, fat, and muscle). We created a compact 2-port MIMO antenna, elliptical microstrip patch antenna elements, and a ground plane on the denim fabric's substrate. This two-port MIMO antenna was designed to work effectively in the 5G sub-6 GHz (3.5 GHz) and WiFi 5.2 GHz frequency bands.

Application of the miniaturization techniques

To achieve the desirable frequency bands, we applied a few miniaturization techniques, such as multiple ground slots in continuity and removing an arched-shaped section and a vertical slit from the elliptical patch. Consequently, asymmetric L-shaped stubs are connected to realize good impedance matching in the intended frequency bands.

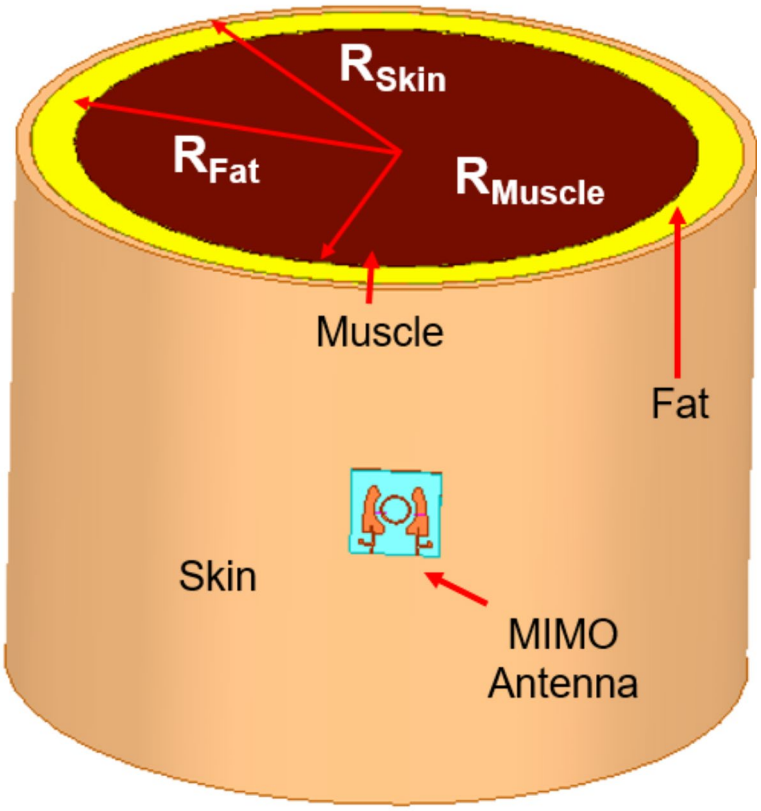

Fig. 3. MIMO antenna on the skin-fat-muscle-layers canonical chest phantom (R_{Skin} = 100 mm, R_{Fat} = 96 mm, R_{Muscle} = 84 mm).

MIMO antenna isolation enhancement

A circular decoupling ring was created between the MIMO's two modified elliptical patch antennas. It assisted in isolation enhancement. The next section provides a thorough explanation of the MIMO antenna evolution.

2-port wearable MIMO antenna's design evolution

Figure 5 describes the evolution of the MIMO antenna design, as explained following:

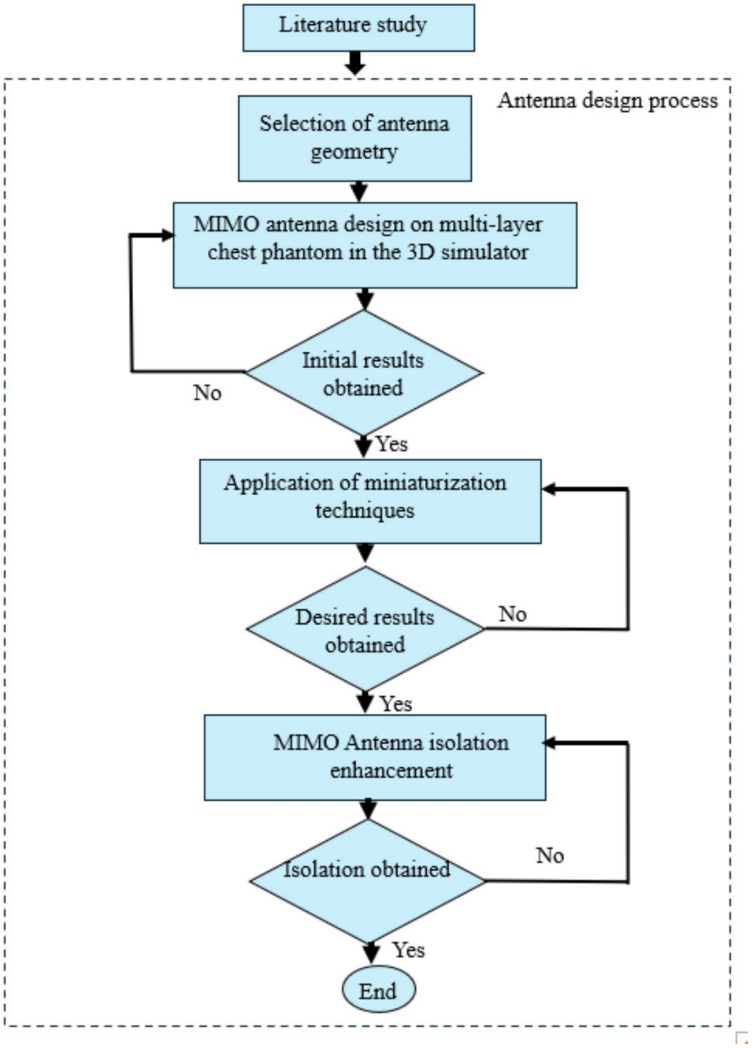

Fig. 4. Proposed wearable MIMO antenna design's technical route.

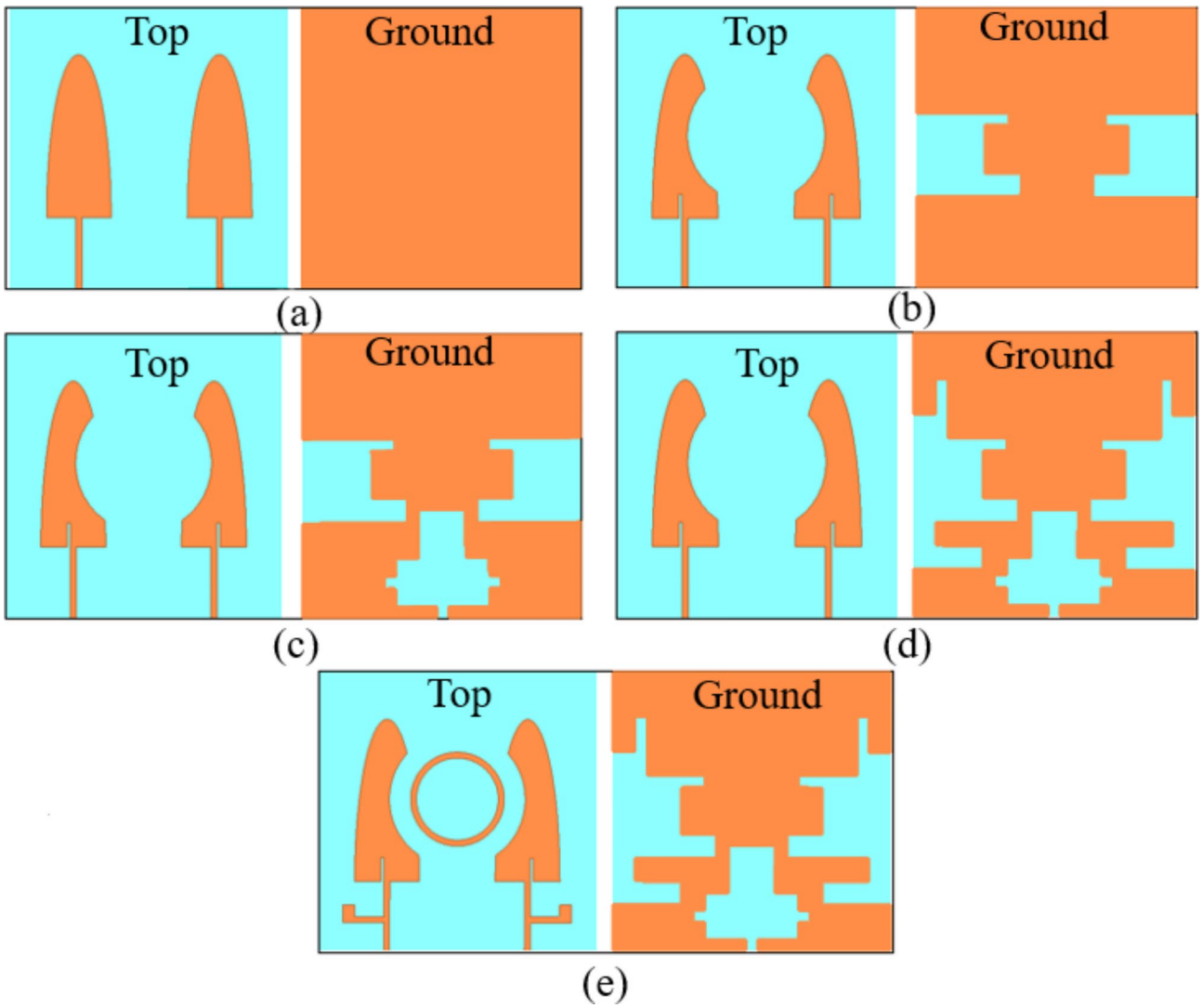

Fig. 5. Evolution of the wearable MIMO antenna design: (**a**) Ant. 0, (**b**) Ant. 1, (**c**) Ant. 2, (**d**) Ant. 3, and (**e**) Ant. 4.

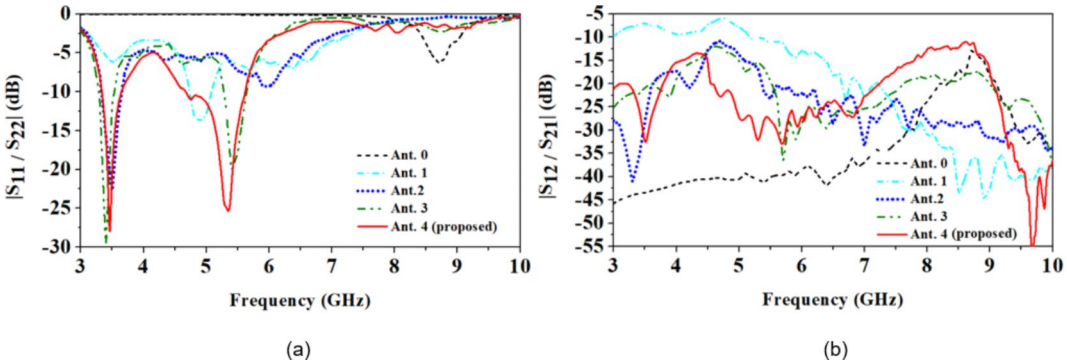

Fig. 6. S-parameters at each stage of the antenna evolution (**a**) S_{11}/S_{22} (**b**) S_{12}/S_{21}.

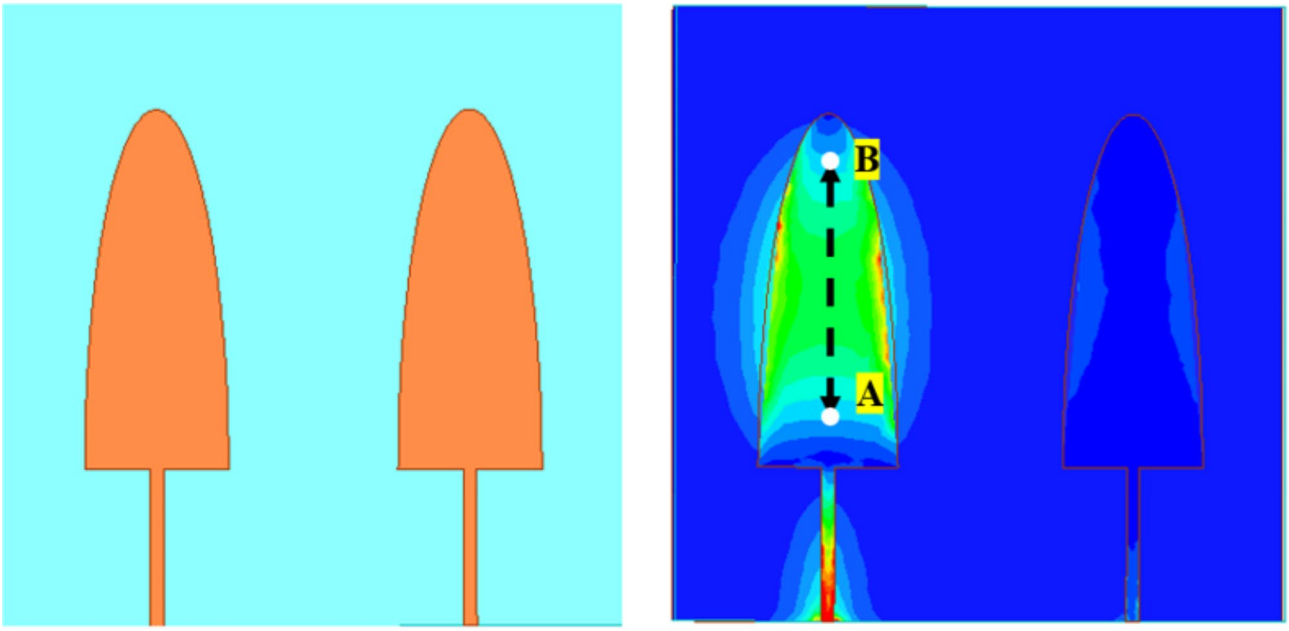

Fig. 7. First step (Ant. 0) of the MIMO Antenna evolution (**a**) Antenna design (**b**) Current distribution.

Ant. 0

In the beginning, Ant. 0 is a simple semi-elliptical microstrip patch antenna with microstrip feed designed on top of the denim substrate with a full ground plane on the backside, as shown in (Fig. 5a). The antenna resonates at 8.7 GHz frequency with 15 dB isolation, as shown in (Fig. 6a,b). Figure 7a, b show design of Ant.0 and its current distribution, respectively.

At 8.7 GHz, the distance between successive current minima AB (λ_g) is 9.65 mm, as shown in (Fig. 7b). The theoretical guided wavelength is calculated from the equation,

$$\lambda_g = \lambda_0/\sqrt{\epsilon_{ra}} \tag{1}$$

where, ϵ_{ra} = permittivity (average permittivity of the denim, air and skin)

λ_0 = free space wavelength.

The calculated value of λ_g from Eq. (1) is 9.5 mm, which is almost the same as the resonating length of the current distribution of Ant.0 of (Fig. 7b). However, matching is not satisfactory in this design step.

Ant. 1

In this step (Ant. 1), to achieve the lower resonance, the current path was increased by removing an arced-shaped section from the elliptical part of the patch antenna and a small slit along the feed length on the elliptical radiating patch, described in (Fig. 5b).

The ground plane of Ant. 1 was also modified by creating two asymmetric U-slots along its length. This change increased the current's path and led to a resonance shift from 8.7 GHz to 4.75 GHz but with poor isolation of 7 dB, as shown in (Fig. 6a,b). One lower resonance was also created at 3.5 GHz, with poor impedance matching, as given in (Fig. 6a,b). We can notice from current distributions in Fig. 8a,b that at 3.5 GHz, the non-curved part of the radiating patch is activated, but the 4.75 GHz resonance is caused by the curved part of the patch, respectively. Also, there is a strong coupling to port 2 of the antenna when only input power is applied to port 1. The subsequent important objective was to enhance port isolation, the impedance matching at the targeted 3.5 GHz, and the tuning of 4.75 GHz to the desirable Wi-Fi 5.2 GHz frequency band.

Ant. 2

Here, in this step (Ant. 2), as shown in (Fig. 5c), the MIMO antenna's elements were kept the same; only the ground plane was modified to achieve isolation between the antenna elements.

Figure 5c describes two rectangular slots (vertical and horizontal) merged with two slits along the length of the merged slots and one slit along the width supported to obtain enhanced port isolation. This change caused the increased current path between the antenna element's ports and enhanced the isolation. This phenomenon is also clear from current distribution plots at 3.5 and 5.8 GHz, as shown in (Fig. 9a,b), respectively. We can also observe from Fig. 9 that the current at the ground plane is confined around the two merged vertical and horizontal rectangular slots. This results in a significant reduction in coupling to port 2, as shown in (Fig. 9).

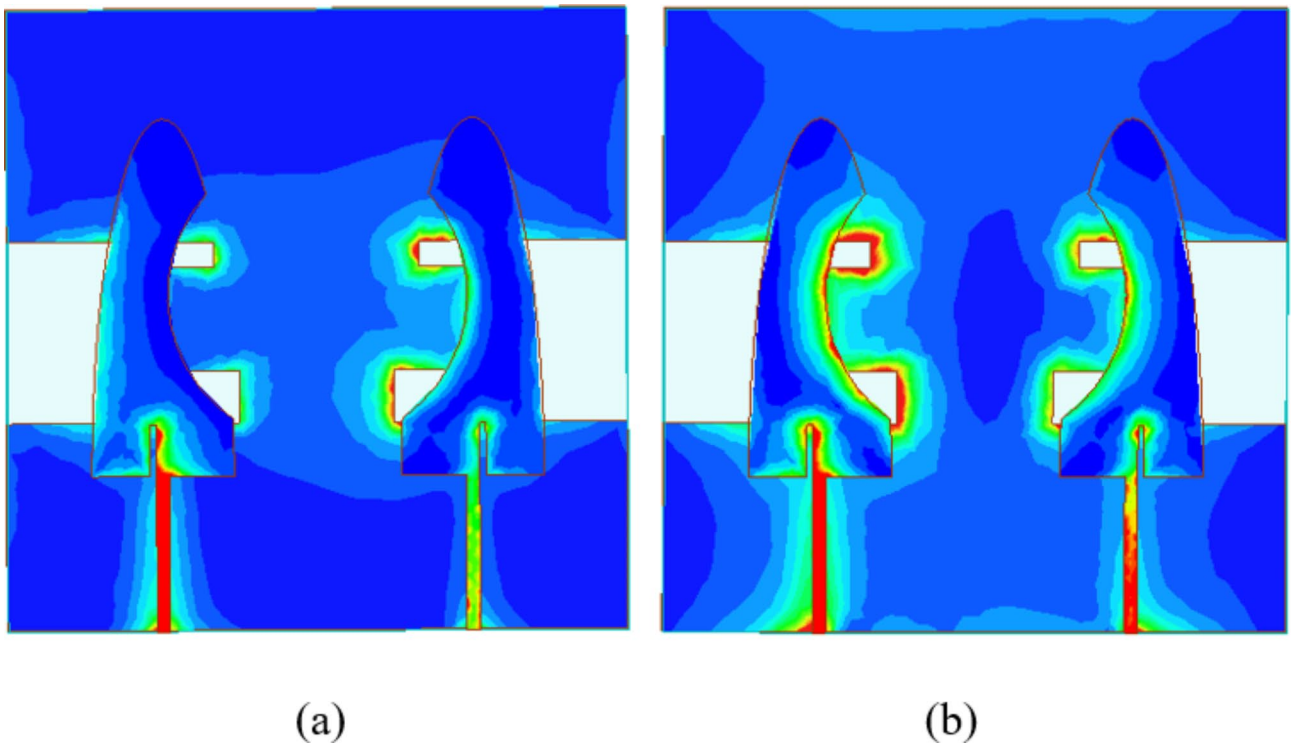

Fig. 8. Second step (Ant. 1) of the MIMO antenna evolution's current distributions at (**a**) 3.5 GHz and (**b**) 4.9 GHz.

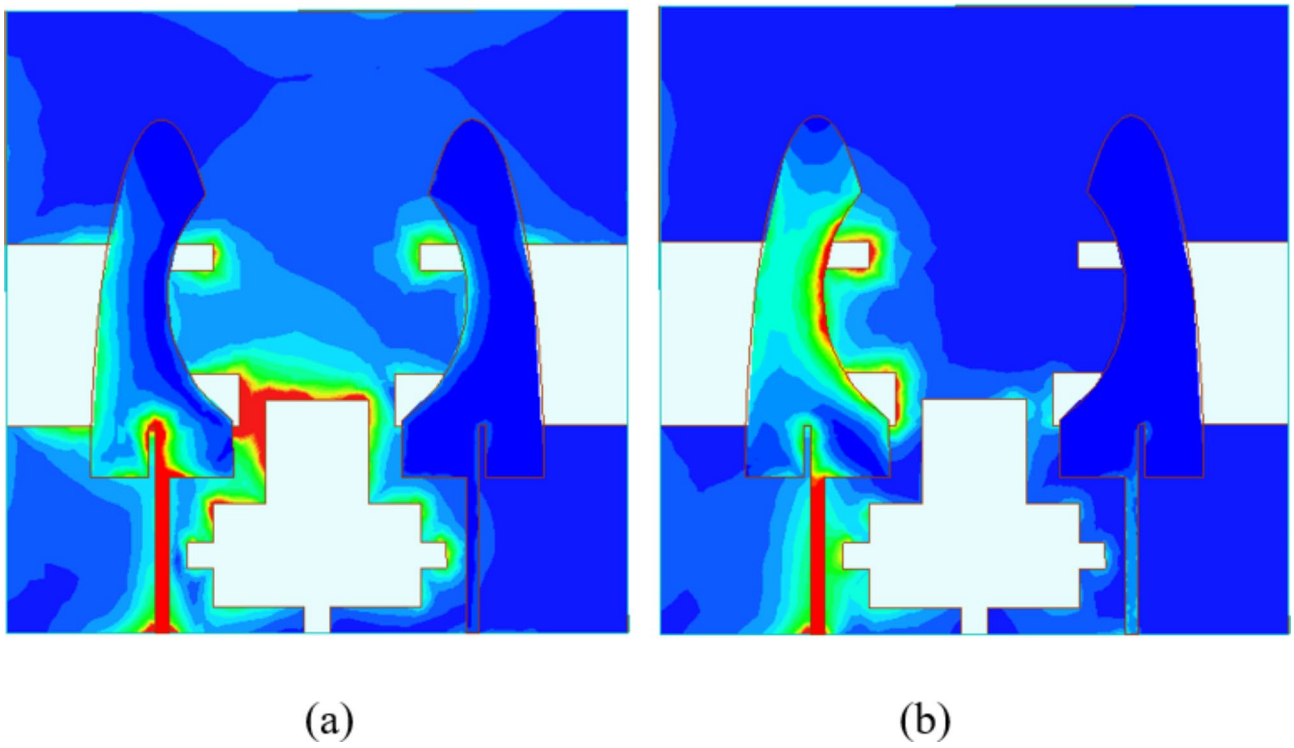

Fig. 9. Third step (Ant. 2) of the MIMO antenna evolution's current distributions at (**a**) 3.5 GHz and (**b**) 5.8 GHz.

Finally, we could achieve good impedance matching at the lower 3.5 GHz resonance and more than 20 dB isolation in both resonances, as illustrated in (Fig. 6a,b), respectively. However, the higher resonance had poor impedance matching.

Ant. 3

In this step, the MIMO antenna's ground plane was further modified by introducing two thin vertical slits (of width L_2) and two horizontal slits (of width W_9), as shown in (Fig. 5d). This modification caused the shifting of resonances from 3.5 to 3.4 GHz and 5.8 to 5.4 GHz due to an increased current path on the ground plane, as shown in (Fig. 10a,b), respectively. However, the impedance bandwidth was reduced.

Ant. 4

In the final step, an L-shaped stub was connected to the microstrip feed of the modified elliptical patches, as indicated in (Fig. 5e). Its size and location were optimized to tune the higher resonance and the wideband behaviour of 950 MHz from 4.65 to 5.6 GHz, and at 3.5 GHz, the bandwidth is 400 MHz (3.3–3.7 GHz). Finally, a circular decoupling ring was placed between the modified elliptical patches, further enhancing the isolation by 5 dB. Finally, we could achieve more than 25 dB port isolation at 3.5 and 5.2 GHz.

Wearable MIMO antenna's current distribution

Figure 11a, b show the current distributions of the pocket-integrated MIMO textile antenna at 3.5 and 5.2 GHz, respectively. It can be viewed that at 3.5 GHz, the current density is high around the merged ground slots and the top patch's vertical slit because both contributes to this resonance, as shown in (Figs. 5b, c and 6). Also, the decoupling ring shows high current density at 3.5 GHz because it contributes to further isolation enhancement at this resonance, as shown in Fig. 6(b) (plot of Ant. 4). In contrast, the top elliptical patch's modified curved edge and ground slits show high current density owing to their involvement in the higher resonance 5.2 GHz tuning and good impedance matching.

Bending analysis of the designed MIMO antenna at different radii

Effect of bending on S-parameters

Wearable antennas function on the human body, which experiences different bending radii due to body movements. This section evaluated the effect of different bending radii (in both the horizontal and vertical planes) on the antenna's S-parameters.

We have considered three different bending radii to analyse the antenna's performance: 8, 10, and 12 mm, as shown in (Fig. 12a–c). The antenna's bending curves the current's path, and as the antenna experiences more bending, a lower side shift of the resonating frequency shift was observed.

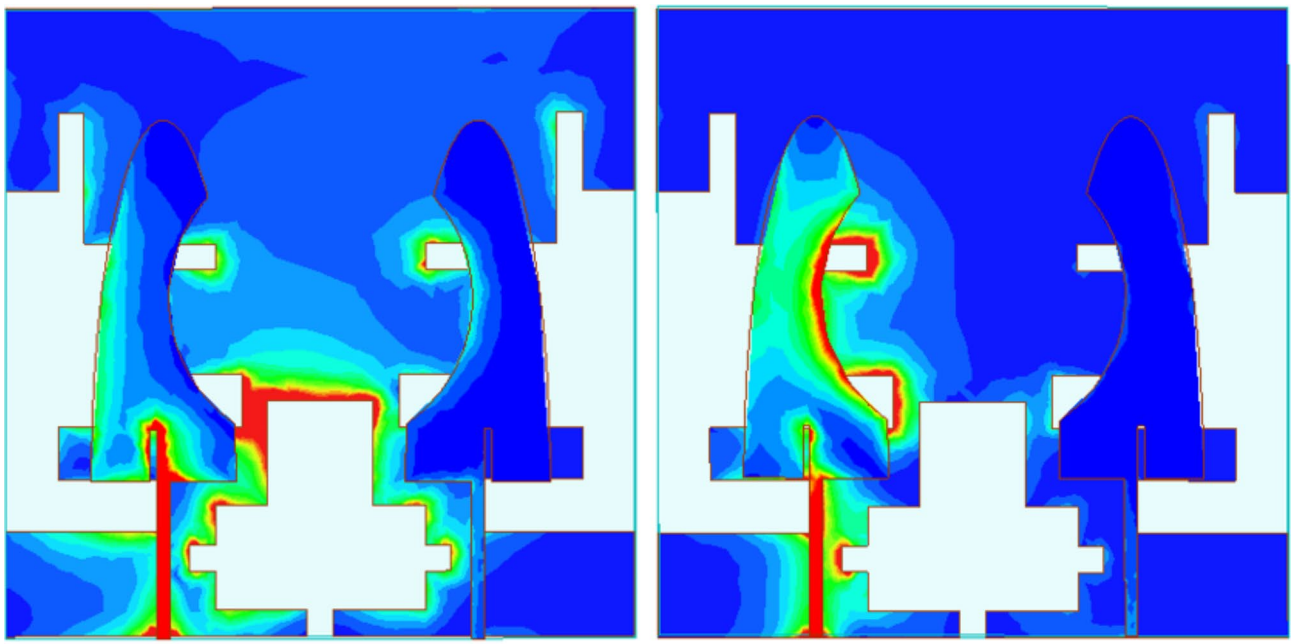

Fig. 10. Fourth step (Ant. 3) of the MIMO antenna evolution's current distributions at (**a**) 3.5 GHz and (**b**) 5.4 GHz.

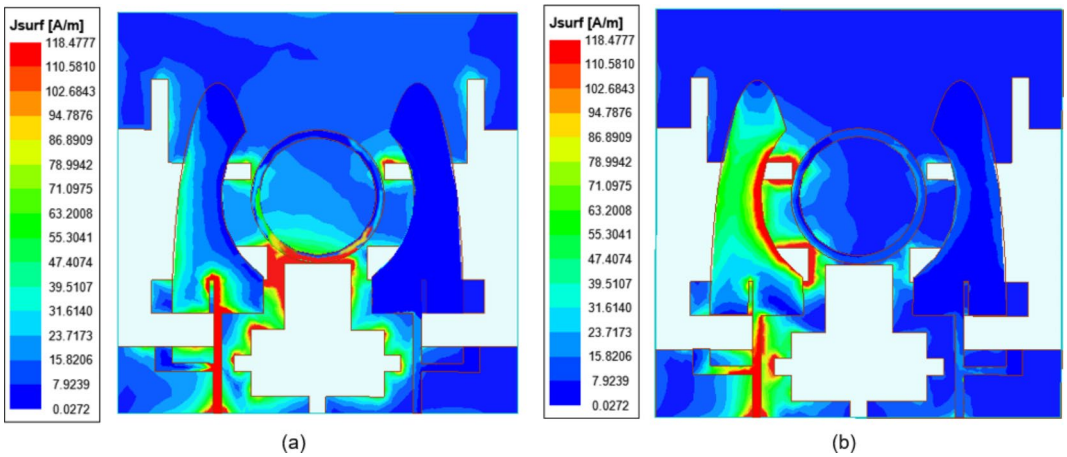

Fig. 11. The current distribution of wearable MIMO antenna at (**a**) 3.5 GHz and (**b**) 5.2 GHz.

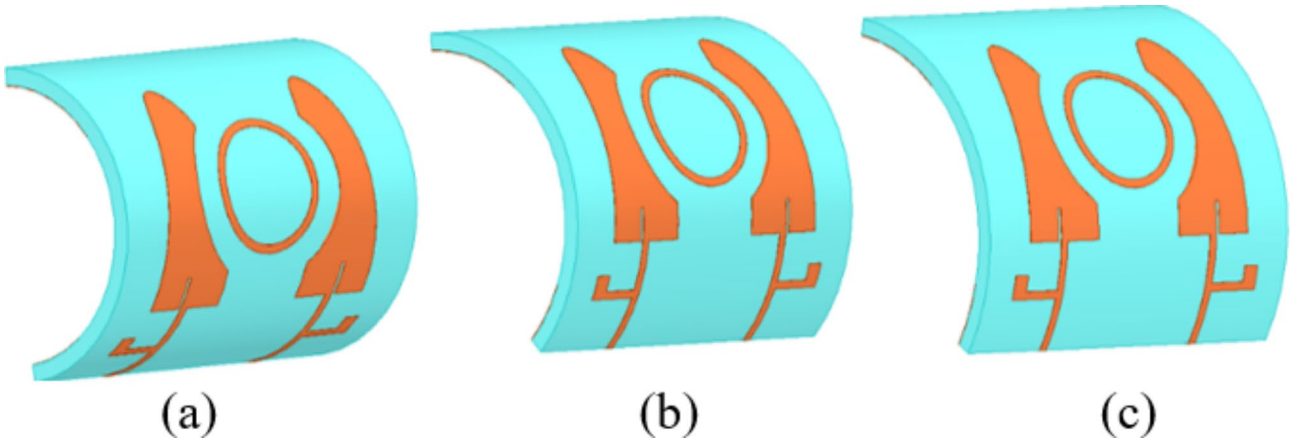

Fig. 12. Bending of MIMO antenna along the X-axis at different radii of (**a**) 8 mm, (**b**) 10 mm, and (**c**) 12 mm.

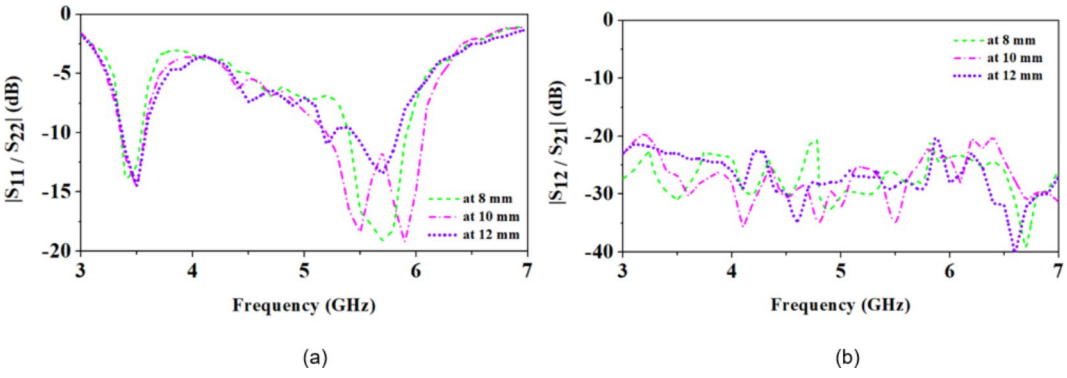

Fig. 13. S-parameters of the MIMO antenna in X-axis bending (**a**) S_{11}/S_{22} (**b**) S_{12}/S_{21}.

As shown in Fig. 12a, when the bending radius was 8 mm, the MIMO antenna's resonating frequencies were shifted to a little lower side at 3.32 GHz (as shown in Fig. 13a) with port isolation > 26 dB (Fig. 13b). However, the higher resonance was at 5.7 GHz with wideband due to the curved current path on the MIMO antenna.

On the other hand, when the bending radius was increased from 8 mm, 10 mm and 12 mm, as indicated in (Fig. 12b,c), the lower resonating frequency was shifted to a slightly higher side of 3.45 GHz, as presented in (Fig. 13b,c). However, at 10 mm and 12 mm bending radius, the modified current path creates two merged resonances and wideband behaviour covering the Wi-Fi 5.2 GHz frequency band, as explained in (Fig. 13b,c).

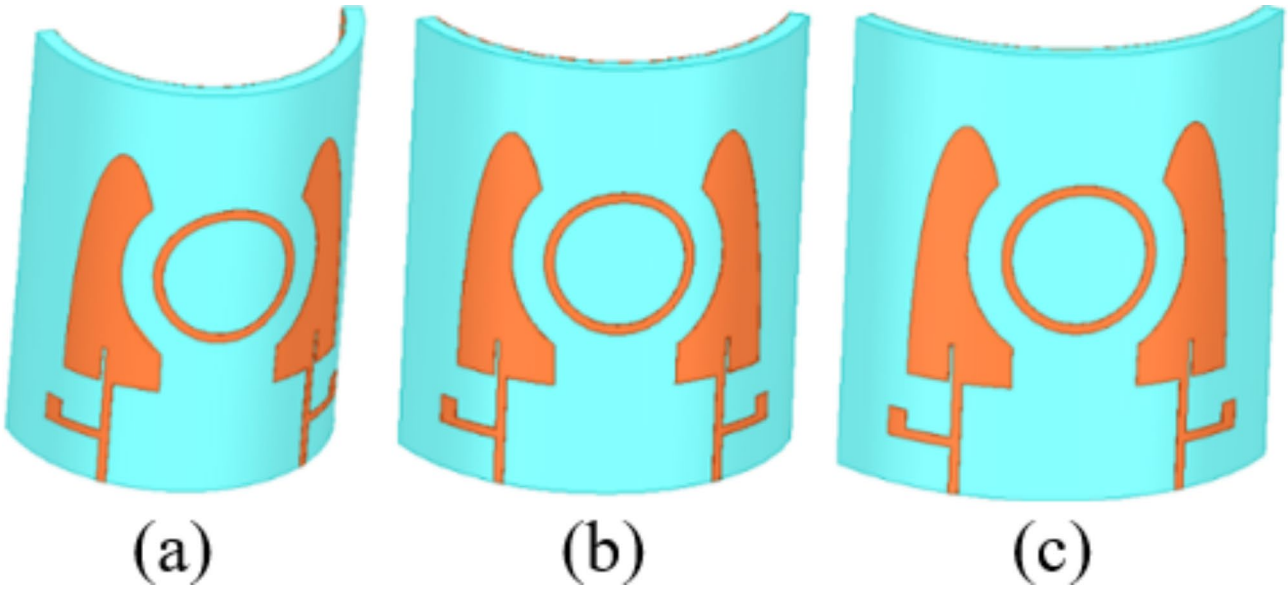

Fig. 14. Bending of MIMO antenna along the Y-axis at different radii of (**a**) 8 mm, (**b**) 10 mm, and (**c**) 12 mm.

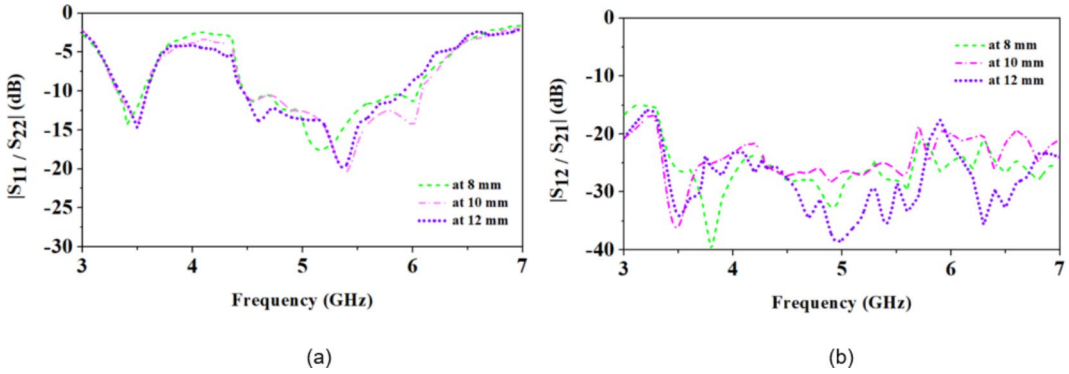

Fig. 15. S-parameters of the MIMO antenna in Y-axis bending (**a**) S_{11}/S_{22} (**b**) S_{12}/S_{21}.

Figure 14a–c indicates the MIMO antenna bending along the Y-axis, and its corresponding S-parameters are given in (Fig. 15a,b). For a maximum bending of 8 mm, the lower resonance frequency is shifted to 3.3 GHz, whereas at 10 and 12 mm bending, the lower resonance frequency is at 3.45 GHz. However, owing to the curved geometry, the higher resonance frequency experiences multiple merged resonances and creates a wideband. The isolation of the MIMO antenna is > 25 dB, and the proposed textile MIMO antenna works well in both frequency bands (3.5 and 5.2 GHz) and can withstand frequency shifts.

Effect of bending on the peak gain of the MIMO antenna

The bending of the MIMO antenna changes its physical form, changing the current distribution along the antenna elements. This can alter the electromagnetic fields around the antenna and modify its radiated power and gain of the antenna. Here, peak gain of the MIMO antenna is examined in the bending in both planes (horizontal and vertical) along the X-axis bending, as illustrated in Fig. 12, antenna's peak gain changed due to the modified current distribution and radiation properties. It can be seen from Fig. 16a that at all the radii of bending along the X-axis, the lower resonance (3.5 GHz) showed more gain (9.5 dBi to 12.7 dBi) than the non-bending state (8.3 dBi). Whereas at the Wi-Fi band of 5.2 GHz, peak gain is 11, 12.5, and 12.95 dBi for bending radius of 8, 10, and 12 mm, respectively. Similarly, bending the wearable MIMO antenna along the Y-axis also causes more gain than the non-bending state. And, at the 5.2 GHz Wi-Fi, this MIMO antenna experiences a gain of 11.5, 12.4, and 13.32 dBi, respectively, as shown in (Fig. 16b).

Effect of bending on the efficiency of the MIMO antenna

Here, we have discussed the effect of bending on the antenna's efficiency at 8, 10, and 12 mm radii.

Figure 17a, b shows that as the bending increases, efficiency reduces rapidly. In the X-plane, with a 12 mm bending radius, efficiency at 3.5 GHz is 68%. Whereas, at 10 mm and 8 mm bending radii, efficiency is 62 and

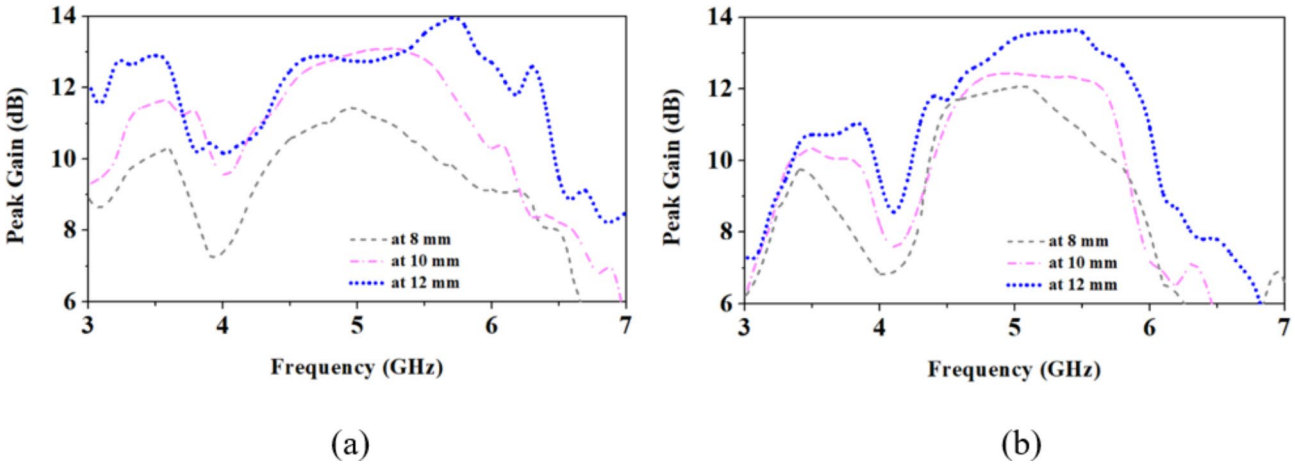

Fig. 16. Peak gain of the MIMO antenna when bending along the (**a**) X-axis and (**b**) Y-axis.

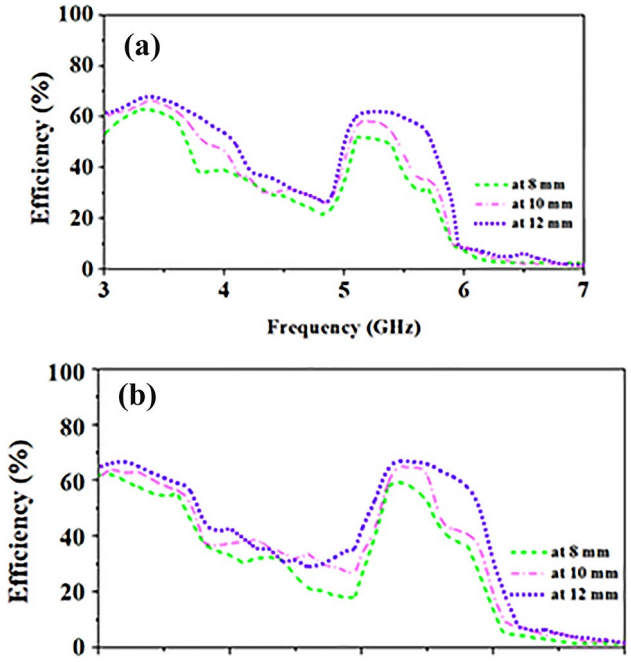

Fig. 17. Efficiency of the MIMO antenna when bending along the (**a**) X-axis and (**b**) Y-axis.

59%, respectively. In the Y-plane, at 12 mm bending radius efficiency at 3.5 GHz is 70%, and at 10 mm and 8 mm bending radii, efficiency is 66 and 60%, respectively.

Effect of maximum bending on S-parameters

In this section, we have discussed the effect of a wearable MIMO antenna's maximum bending (along the X-axis and Y-axis), current distributions, and corresponding S-parameters in Figs. 18 and 19, and Fig. 20, respectively. The extreme bending radius at which the MIMO antenna doesn't perform well is 5 mm radius. Figure 20a shows that the bending of the MIMO antenna shifts the lower resonance of 3.5 to 3.35 GHz and 3.3 GHz for X-axis and Y-axis bending, respectively. However, the upper resonance of 5.2 GHz has disappeared. Also, the isolation between the antenna elements has deteriorated and caused strong coupling, as given in (Fig. 20b). The reason for these changes is the deformation of the antenna geometry. It introduces a capacitance C_B due to the closeness of two opposite sides of the MIMO antenna, as shown in (Fig. 19a,b). This capacitance has a large value as compared to the larger bending radius due to the reduced distance between the opposite sides of the ground planes. We know that the capacitance is opposite to the frequency, i.e. $X_c = {}^{1}\!/_{2\pi fC}$. This large

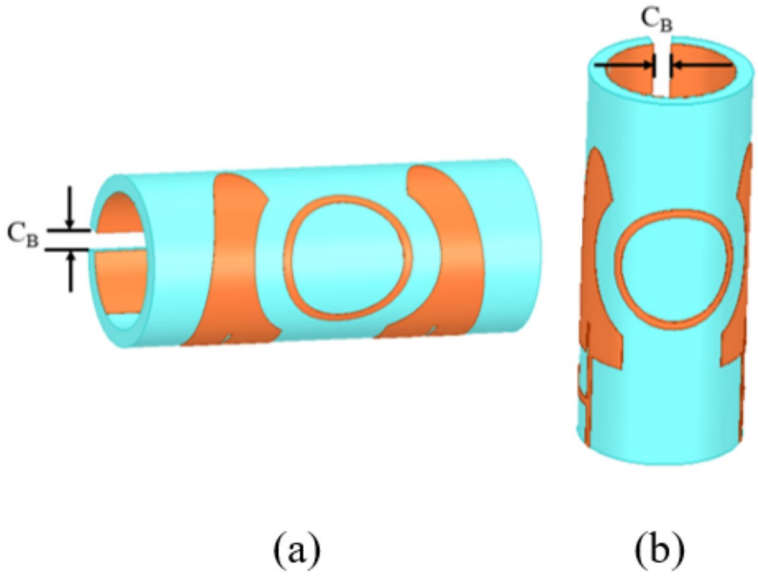

Fig. 18. Extreme bending of the proposed MIMO antenna at 5 mm bending radius along the (**a**) X-axis (**b**) Y-axis.

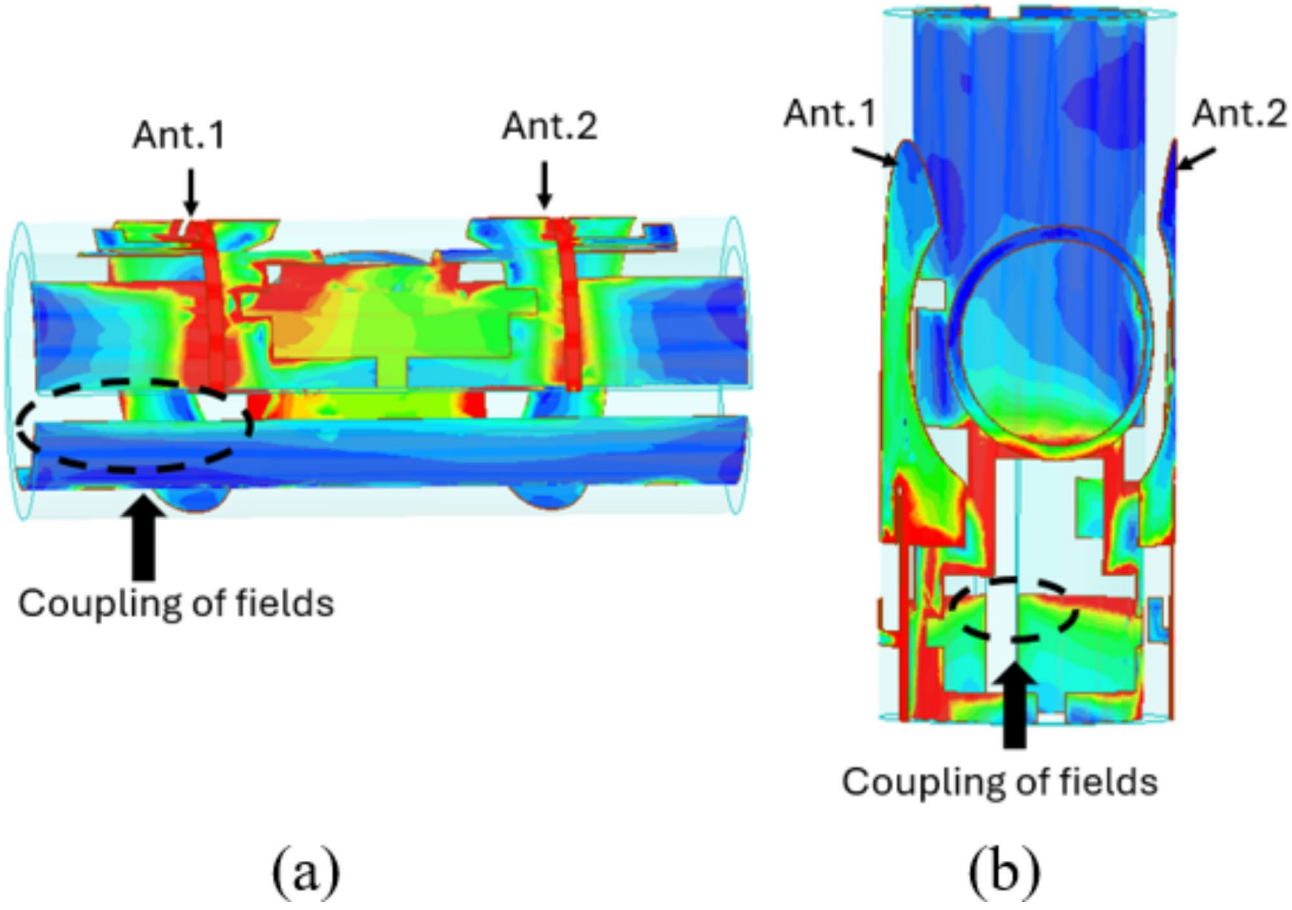

Fig. 19. Current distributions indicate strong coupling of fields from the ground plane in extreme bending of the proposed MIMO antenna (**a**) along the X-axis (**b**) and Y-axis.

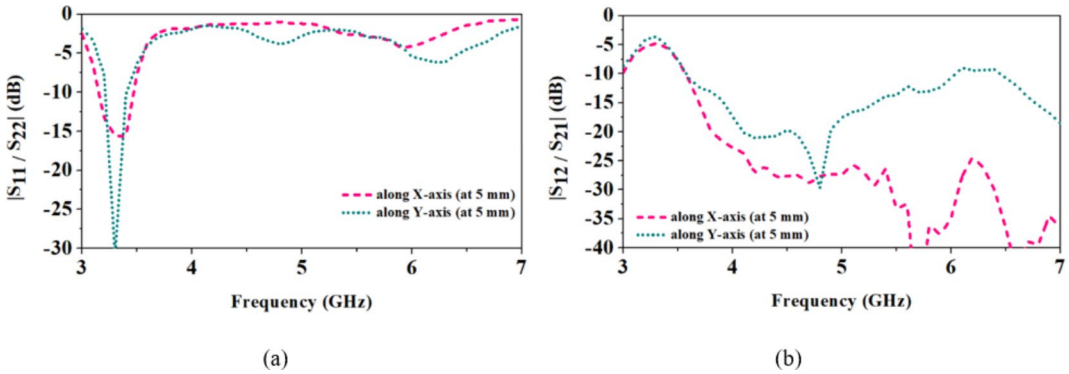

Fig. 20. S-parameters of the MIMO antenna in maximum bending (along the X-axis and Y-axis) (**a**) S_{11}/S_{22} (**b**) S_{12}/S_{21}.

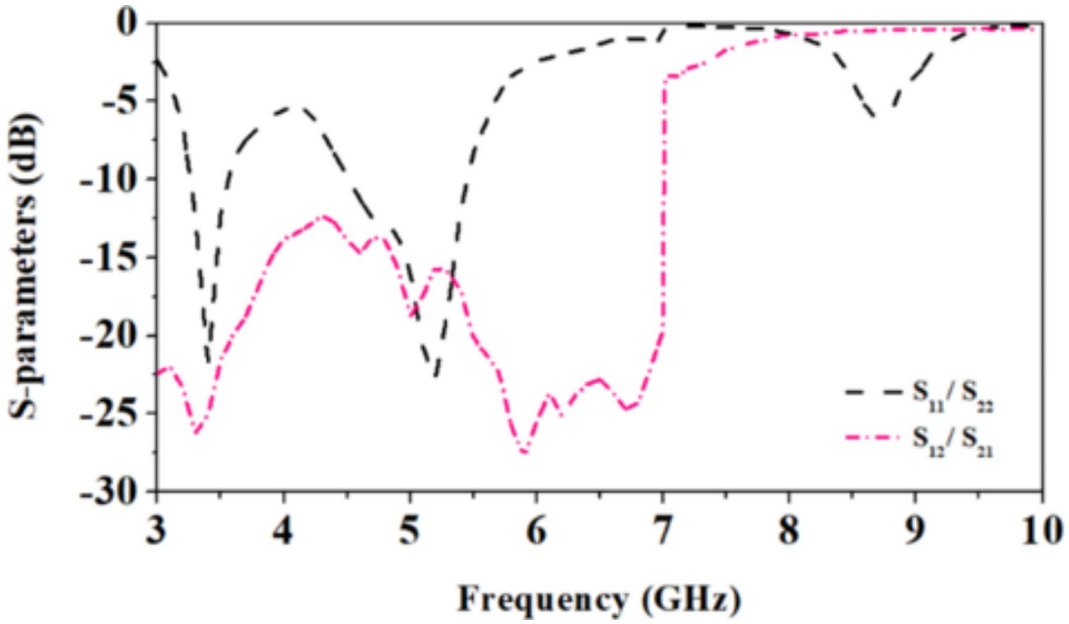

Fig. 21. Effect of waterproofing on the S-parameters of the proposed MIMO antenna.

value capacitance detunes the higher frequency band, as shown in (Fig. 20a,b). The poor isolation in the extreme bending scenario is due to the strong coupling between the antenna elements due to the closeness of the opposite edges of the MIMO antenna, as shown in (Fig. 19a,b).

Effect of waterproofing on MIMO antenna's performance

It is a well-known fact that humidity and sweat can cause the antenna to detune due to the water content absorbed in the fabric. Since water has a high dielectric constant ($\varepsilon_r = 80$), it will deteriorate the antenna's performance. To avoid such situations, wearable antennas can be waterproofed. Plastic waterproof materials have a low dielectric constant ($\varepsilon_r = 2$) and can keep the antenna free from detuning due to the moisture from sweat/humidity. Figure 21 shows the S-parameters due to the waterproofing layer, and it can be seen that the lower value of the waterproof plastic layer did not impact much; the antenna still covers both the resonating frequency bands well.

Effect of human body size on MIMO antenna's performance

This section discusses the impact of human body size on the S-parameters of the proposed MIMO antenna. In the proposed work, we have considered the average human chest size and radius of approximately 100 mm. We can observe from Fig. 22a that the 50 ohm impedance is slightly shifting to the lower side for smaller body sizes. However, as the human body size increases, the amount of fat increases and the effect of its low dielectric properties causes the antenna to resonate at slightly higher frequencies and cause impedance curves to shift to a higher side. However, in both cases, the antenna effectively covers the reported 3.5 and 5.2 GHz frequency bands with close to the 50 ohm impedance. The gain of the MIMO antenna is impacted by the larger body sizes, as shown in (Fig. 22b). When the human body chest phantom size is smaller than the average standard size

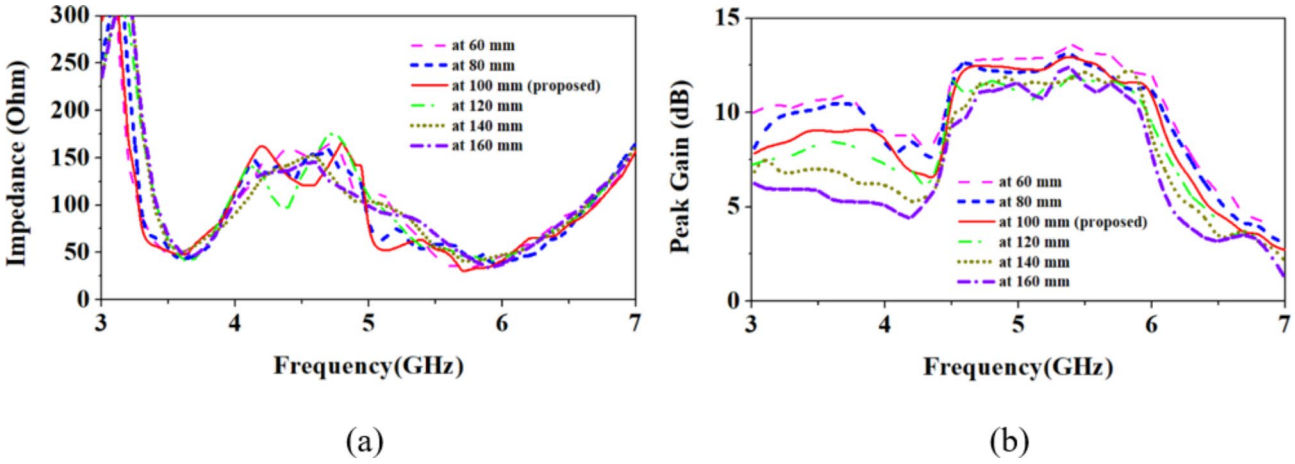

Fig. 22. Effect of human body size on (**a**) Impedance and (**b**) Gain of the proposed MIMO antenna.

(100 mm), the MIMO antenna experience improved gain values of 10.1 and 9.7 dBi at 60 and 80 mm radius of cylindrical chest phantom, respectively, at 3.5 GHz. On the other hand, when the chest radius becomes 120, 140, and 160 mm, gain values become 8.6, 7.72, and 6.4 dBi, respectively, at 3.5 GHz. At higher resonance, at 60 and 80 mm chest radius, gain is 13.8 and 13.1 dBi, respectively, slightly higher than the standard chest size of 100 mm (proposed). The minimum gain value at the chest phantom radius of 160 mm is 11.2 dBi, which is almost 2 dBi less than the proposed MIMO antenna's gain. Here, we can notice that the proposed MIMO antenna works well at different chest sizes of the human body with optimum gain values.

Effect of multiple fabric layers on MIMO antenna's radiation patterns

In this section, we have evaluated the effect of the thickness or layers of clothes on the antenna's radiation patterns. The clothes' layers/thickness impact the E-plane and H-plane gains, as shown in (Fig. 23). When the thickness of the fabric is 2 mm and 4 mm, the H-plane co-polarized gain in the boresight direction becomes 6.2 and 6.5 dBi, respectively. However, the 6 mm cloth thickness caused little improvement and caused it 7 dBi, in boresight direction, at 3.5 GHz. But, as the thickness is 8 mm, the co-polarized gain drops and becomes 3.88 dBi. It can also be noticed that in the E-plane, the gain is more directive at thick-layer fabrics, as depicted in (Fig. 23).

Effect of bending on MIMO antenna's radiation patterns

The bending of the MIMO antenna changes its physical form, changing the current distribution along the antenna elements. This can alter the electromagnetic fields around the antenna and modify its radiated power and directional properties, as depicted in (Fig. 24). The antenna experiences tilt in the radiation patterns (at 10 and 12 mm bending radii). Still, more bending causes an unstable radiation pattern (at 8 mm bending radii), as shown in (Fig. 24a–d). Not only tilted radiation patterns but gain also drops quickly (6 and 4.3 dBi in H-plane and E-plane, respectively) as the bending radii reduce to 8 mm at 3.5 GHz resonance. At 5.2 GHz resonance, the H-plane and E-plane's maximum values are 5.5 and 8.45 dBi at 8 mm bending radii.

Fabrication and measurement

In the proposed work, the fabrication technique to realize the textile antenna used a flexible adhesive copper sheet (24 mm wide and 0.065 mm thick) and a cutting plotter to shape and cut the patch and the ground plane[29]. This is a widely used, cost-effective, and time-saving fabrication technique. Also, an antenna with copper tape material demonstrates improved radiation efficiency and gain[30].

Measurement of S-parameters of the proposed pocket-integrated compact and dual-band MIMO antenna

The reported antenna is created on the denim textile, and its prototype is given in (Fig. 25). The antenna's top has two modified elliptical antenna elements with L-shaped stubs and a decoupling ring to improve their isolation, as indicated in (Fig. 26a). A slot-loaded ground plane is at the backside of the MIMO antenna, as shown in (Fig. 26b), and the VNA (vector network analyzer) used to measure S-parameters is shown in (Fig. 26c). The fabricated prototype of the proposed compact dual-band MIMO antenna is seamlessly integrated with the shirt's pocket.

When the MIMO antenna is integrated outside the pocket, as presented in (Fig. 26a), the low resonant frequency shifts to the lower side, as shown in (Fig. 27a); in this situation, simulated and measured values of the MIMO antenna are 3.3 GHz and 3.43 GHz, but it still effectively covers the sub-6 3.5 GHz frequency band. However, the upper-frequency band resonates at 5.6 GHz in the HFSS simulator and at 5.3 GHz during measurement. The reason for this change is the large actual human body size in measurement compared to the multi-layer canonical phantom used in the simulator because it is not possible to simulate the actual human body-sized phantom in the simulator. The heterogeneity and complexity of the human body's dielectric properties cause frequency shifts. Also, fabrication tolerances and measurement depth inside the phantom/pork

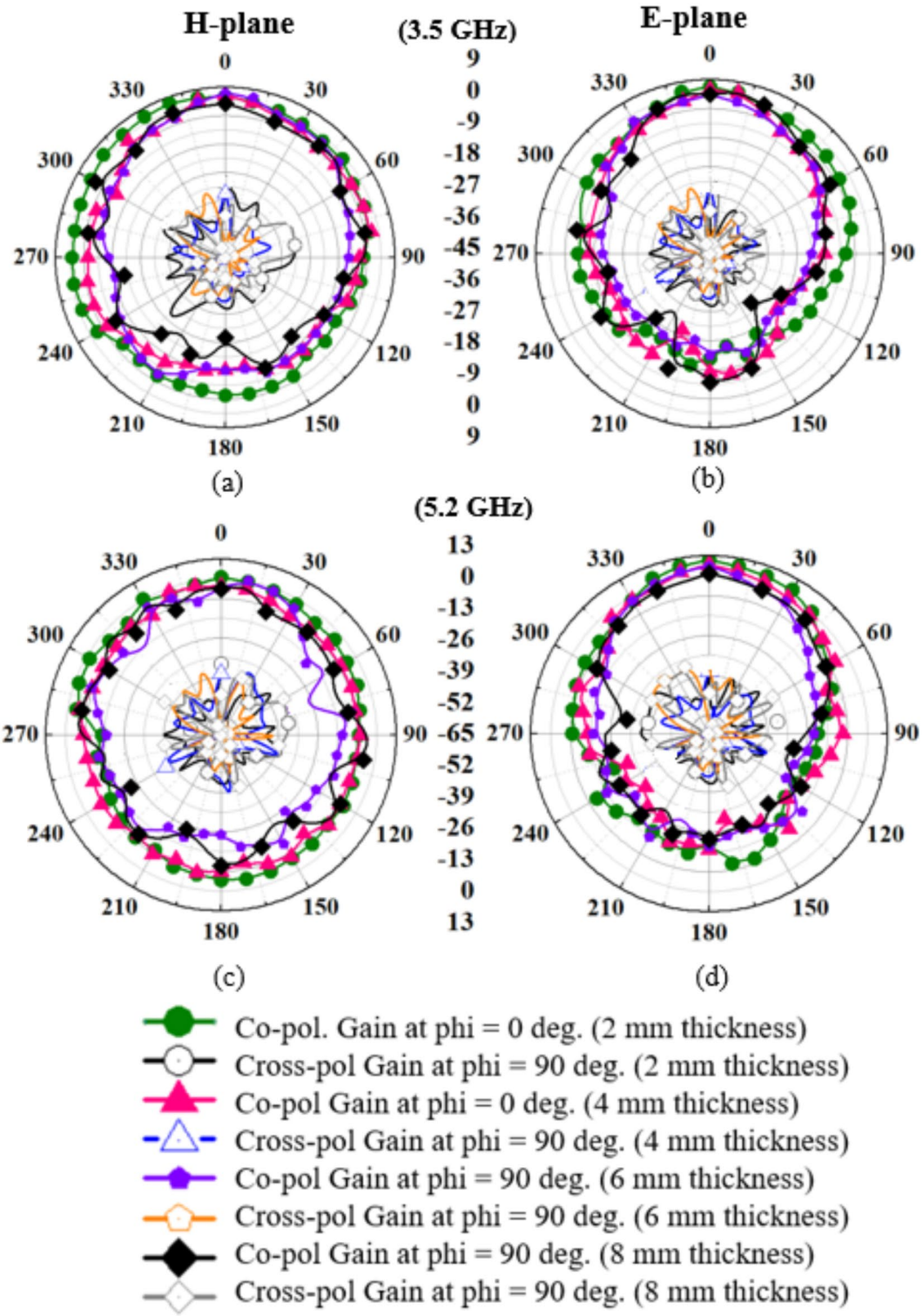

Fig. 23. Simulated radiation patterns at different thickness of the layers (2, 4, 6, 8 mm): (**a**) *H*-plane (at 3.5 GHz), (**b**) *E*-plane (at 3.5 GHz), (**c**) *H*-plane (at 5.2 GHz), (**d**) *E*-plane (at 5.2 GHz).

are crucial factors affecting the antenna's response during measurements. We have carefully considered these factors in our proposed work to avoid inconsistencies. It can be noted that it shifted to a higher side than the inside pocket antenna due to the fabric layer on the top of the antenna's copper, as shown in (Fig. 27a). The port isolation in both cases is quite good (≈ 25 dB), as shown in (Fig. 27b).

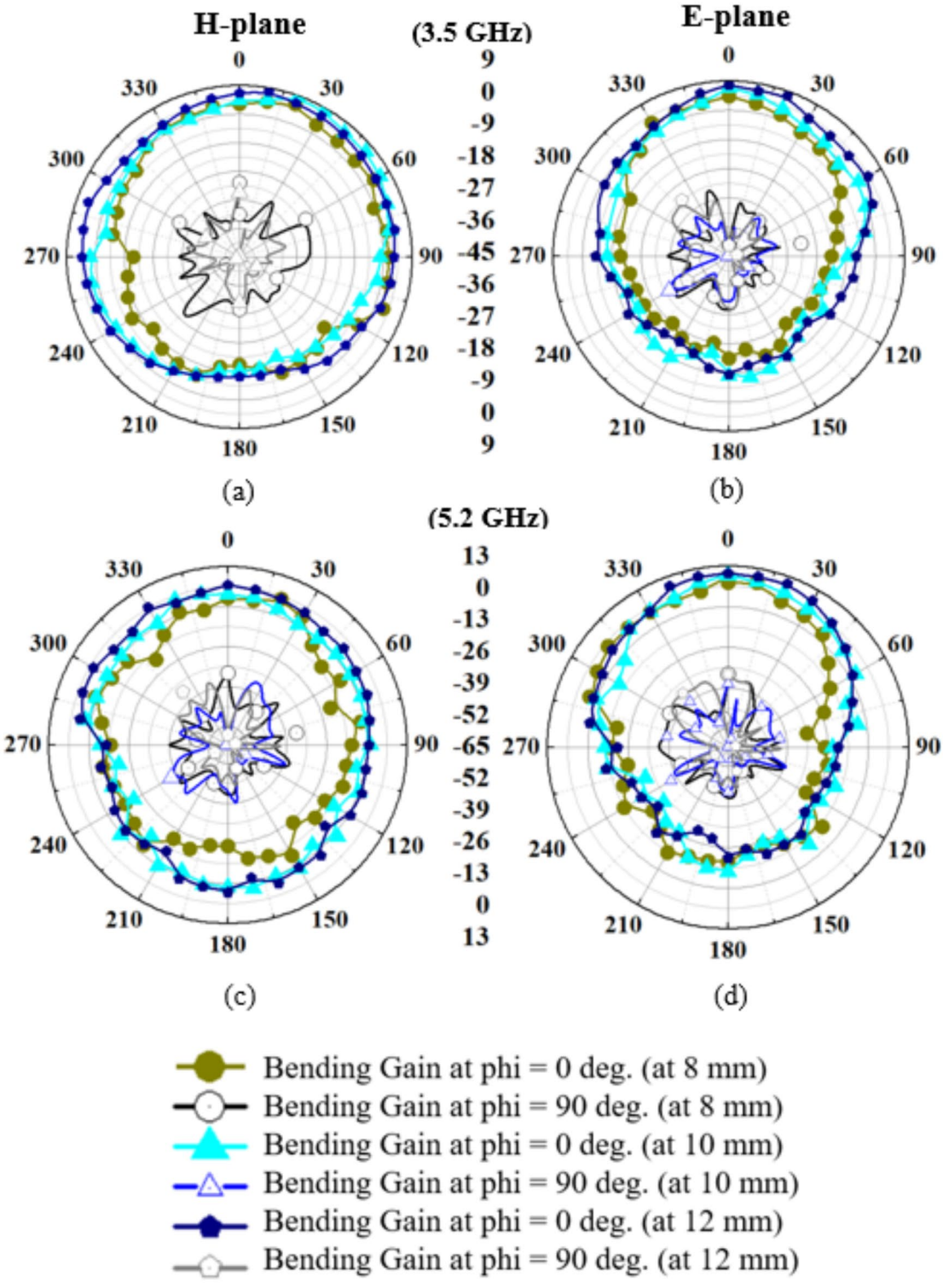

Fig. 24. Simulated radiation patterns at different thickness of the layers (2, 4, 6, 8 mm): (**a**) *H*-plane (at 3.5 GHz), (**b**) *E*-plane (at 3.5 GHz), (**c**) *H*-plane (at 5.2 GHz), (**d**) *E*-plane (at 5.2 GHz).

Far-field measurement

A comparison between gains during simulation and measurement is indicated in (Fig. 28 and in Table 2). At 3.5 and 5.2 GHz frequencies, radiation patterns in the *H*-plane and *E*-plane at $\phi = 0^{\circ}$ are close to omnidirectional, as illustrated in (Fig. 28a–d). This textile MIMO antenna is radiating outside chest due to the boresight pattern in both simulated and measured state.

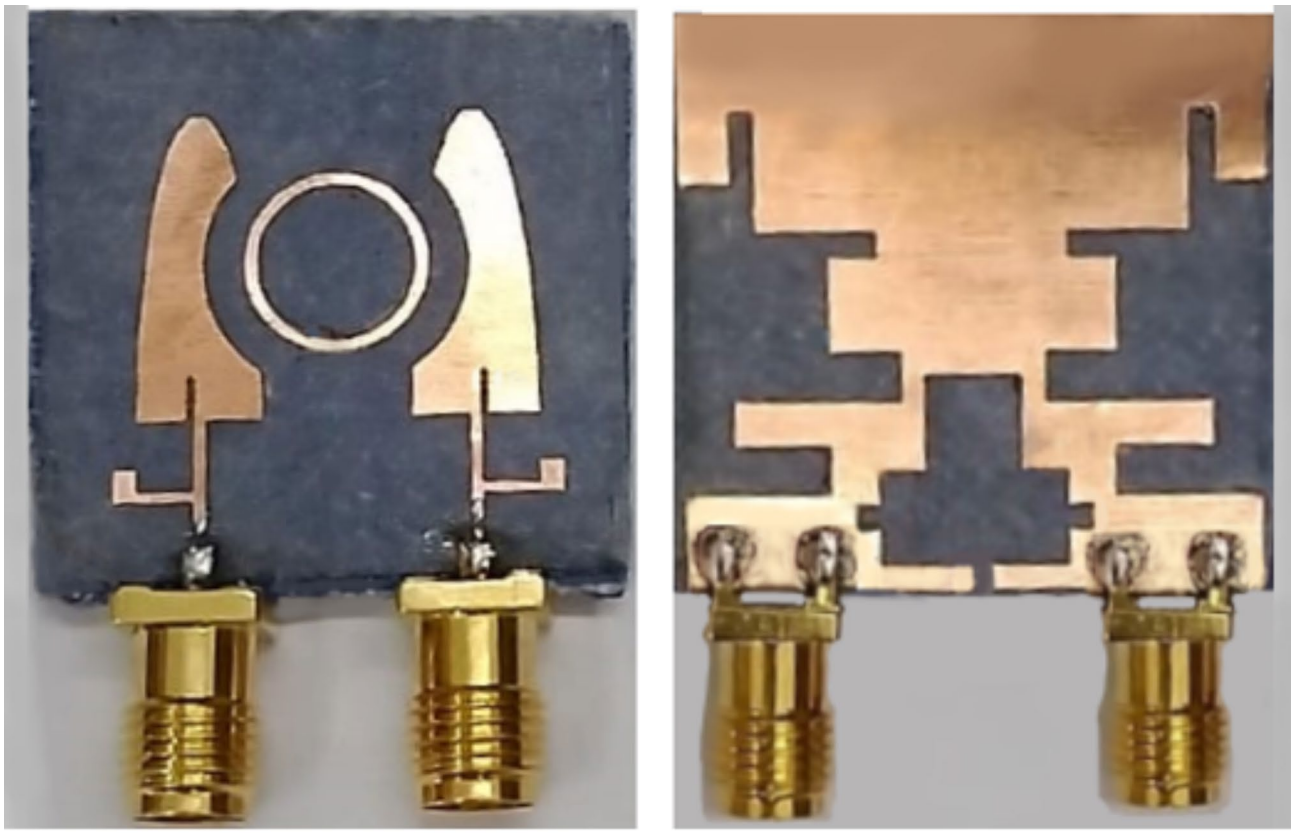

Fig. 25. Fabric fabricated textile MIMO antenna prototypeated prototype of the antenna: (**a**) modified elliptical patch elements and (**b**) ground plane with continuous slots.

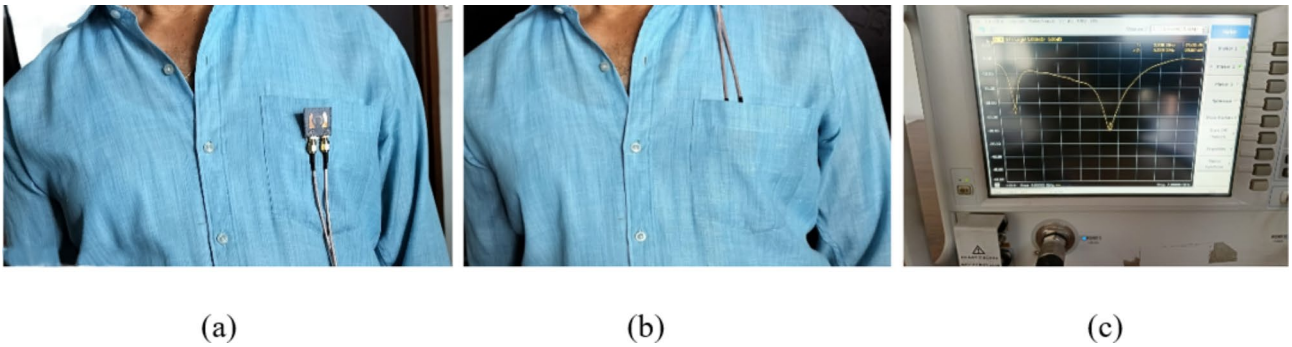

Fig. 26. Proposed antenna measurement is (**a**) visible position, (**b**) hidden position, and (**c**) VNA measurement.

Simulated vs measured efficiency

The maximum simulated radiation efficiency of the MIMO antenna is 72 and 71.6% for the 3.5 GHz and 5.2 GHz frequency bands, respectively. The radiation efficiency measured is slightly lower owing to the small human chest (Table 3) and the heterogeneity of the human body, which causes losses. We can observe from Fig. 29 that the measured maximum values of the radiation efficiency are 63.4 and 68.1%, respectively.

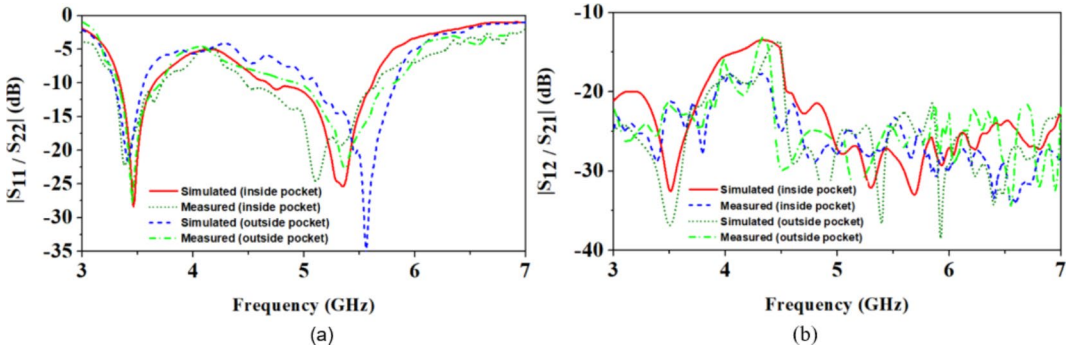

Fig. 27. Simulated Vs measured S-parameters of the proposed antenna (**a**) reflection coefficients and (**b**) transmission coefficients.

Envelope correlation coefficient (ECC) and diversity gain (DG)

The correlation between the antenna elements defines the diversity of the MIMO antenna, and ECC is used to estimate it. In a given MIMO antenna system, it identifies the correlation between the nth and the mth radiating elements and they should not have any correlation. But practically, ECC < 0.5 is the upper limit. The ECC is estimated using Eq. (2)[31],

$$ECC_{nm} = \frac{\left| \int_0^{2\pi} \int_0^{\pi} \left[XPR.E_{\theta\, n} E^*_{\theta\, m} p_\theta + XPR.E_{\varphi\, n} E^*_{\varphi\, m} p_\varphi \right] d\Omega \right|^2}{\int_0^{2\pi} \int_0^{\pi} \left[XPR.E_{\theta\, n} E^*_{\theta\, n} p_\theta + XPR.E_{\varphi\, n} E^*_{\varphi\, n} p_\varphi \right] d\Omega \times \int_0^{2\pi} \int_0^{\pi} \left[XPR.E_{\theta\, m} E^*_{\theta\, m} p_\theta + XPR.E_{\varphi\, m} E^*_{\varphi\, m} p_\varphi \right] d\Omega} \quad (2)$$

In Eq. (2), the cross-polarization ratio *XPR* is the average power along coordinates *θ(pV)* and *φ(pH)*. $E_{\theta n}$ and $E_{\varphi m}$ are the complex envelopes along θ and φ direction of the field patterns. The power is fed to the port of n^{th} elements with others at 50 Ohm matched termination.

$XPR = pV/pH = 1$ and p_θ and $p_\varphi = 1/4\pi$, where p_θ and p_φ are the probability distribution of incident power antenna in θ and φ directions, respectively. As indicated in Fig. 30a, in the 3.5 and 5.2 GHz bands, the maximum values of simulated ECC are 0.006 and 0.002, respectively. The measured values in the 5G sub-6 3.5 GHz and Wi-Fi 5.2 GHz bands are 0.015 and 0.013, respectively. Therefore, it can be noted that all the values (simulated and measured) of ECC are below the standard value of ECC, which is 0.5.

Likewise, diversity gain (DG) is crucial in evaluating the performance of the MIMO system. The DG estimates the effect of the diversity scheme on transmitted power. Preferably, it must be 10 dB, which indicates the zero correlation amongst the elements of the MIMO antenna, and estimated by using Eqs. (3),

$$\boldsymbol{DG} = 10\sqrt{1 - (\boldsymbol{ECC}^2)} \quad (3)$$

Figure 30b shows the diversity gain's simulated and measured values are close to 10 dB.

Total reflection coefficient (TARC)

The total active reflection coefficient (TARC) links the total incident power to the total radiated power of the MIMO system. To compute TARC, different ports of the multi-antenna system are fed with different signal phases varying from 0 to 180^0, with a step size of 30^0. We have considered the equations mentioned[32] to evaluate TARC. Figure 31 shows that the behaviour of the MIMO antenna is unaffected by the signal's phase change.

Channel capacity loss (CCL)

Channel capacity loss (CCL) is a crucial parameter for MIMO systems that predicts the maximum information that can be transmitted with minimum losses in the communication channel. A MIMO system's standard channel capacity loss value is less than 0.4 bits/s/Hz. In our proposed work, we can observe that the values of CCL for the proposed frequency bands are below 0.3 bits/sec/Hz, as shown in (Fig. 32).

SAR analysis

When designing an antenna for wearable applications, SAR is a vital parameter. It gives details of the quantity of absorbed power by biological tissues during the antenna's on-body functioning. Corresponding to FCC and ICNIRP standards, the biological tissue of 1 gm and 10 gm cube must not absorbed power > 1.6 and 2.0 W/kg, respectively. Figure 33 describes the 1 gm/10 gm SAR values at 3.5 GHz and 5.2 GHz. When 0.5 W of input power is equally fed to both of the MIMO antenna's ports, the 1 gm/10 gm SAR values at 3.5 and 5.2 GHz are 0.034/0.057 and 0.026/0.0132 W/kg. Table 4 indicates that the recommended wearable textile MIMO antenna has significantly minimal SAR values, demonstrating its harmless use for wearable applications. Here, a total input power of 0.5 W (0.25 W on each port) is fed to the MIMO antenna, which estimates SAR values relatively smaller than the standard values. Also, the wearable devices require power in the range of μW to mW (< 200 mW)[33], and our proposed antenna can easily handle power of 500 mW. Consequently, it concludes the safety of the human body while communicating with external devices.

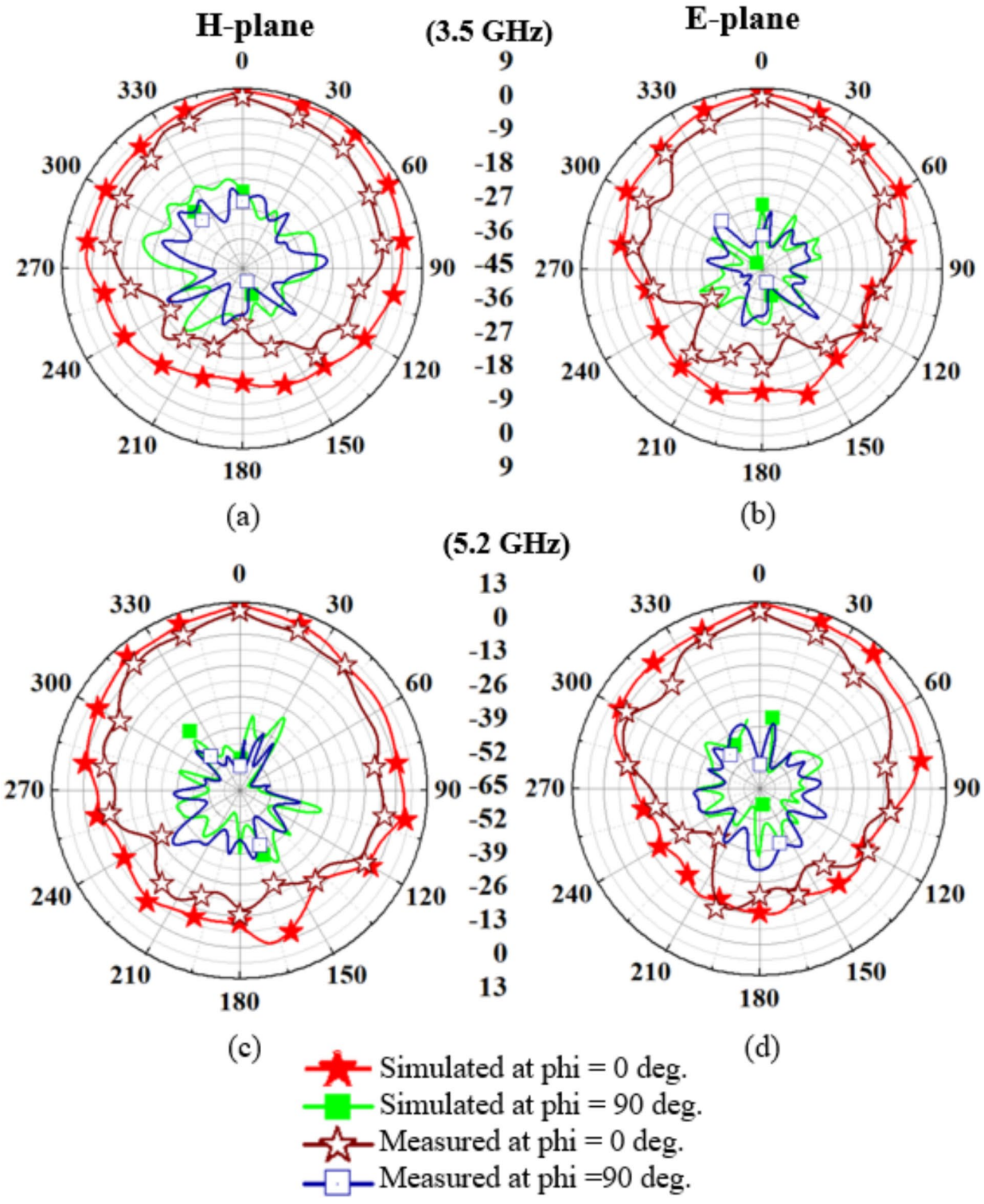

Fig. 28. Simulated Vs measured radiation patterns: (**a**) *H*-plane (at 3.5 GHz), (**b**) *E*-plane (at 3.5 GHz), (**c**) *H*-plane (at 5.2 GHz), (**d**) *E*-plane (at 5.2 GHz).

Link budget analysis (for hidden and visible positions of the wearable antenna)

This work shows the proposed wearable antenna communicating in hidden and visible positions. Figure 34 shows the communication set-up for the antenna hidden inside the shirt's pocket, and Fig. 35 shows the corresponding link margin. Figures 36 and 37 also show the communication setup and the corresponding link margin for the antenna placed outside the shirt's pocket. The external antenna considered in both communications has a gain of 5 dBi, and other parameters to evaluate the link margin are given in (Table 5). A communication link is estimated

Frequency (GHz)	Simulation (chest phantom) (dBi)	Measured (on human chest) (dBi)
3.5	8.3	7.9
5.2	13.0	12.2

Table 3. Simulated and measured peak gain values.

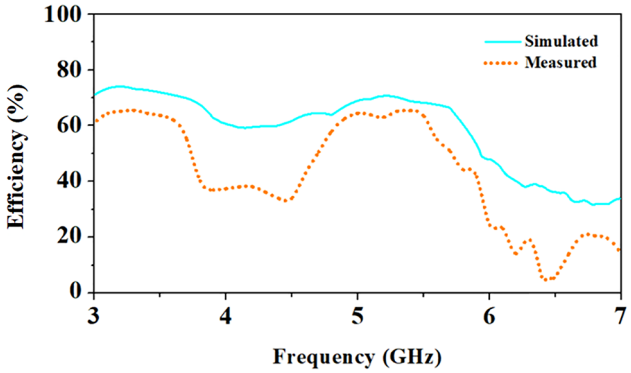

Fig. 29. Simulated Vs radiation efficiency of the MIMO antenna.

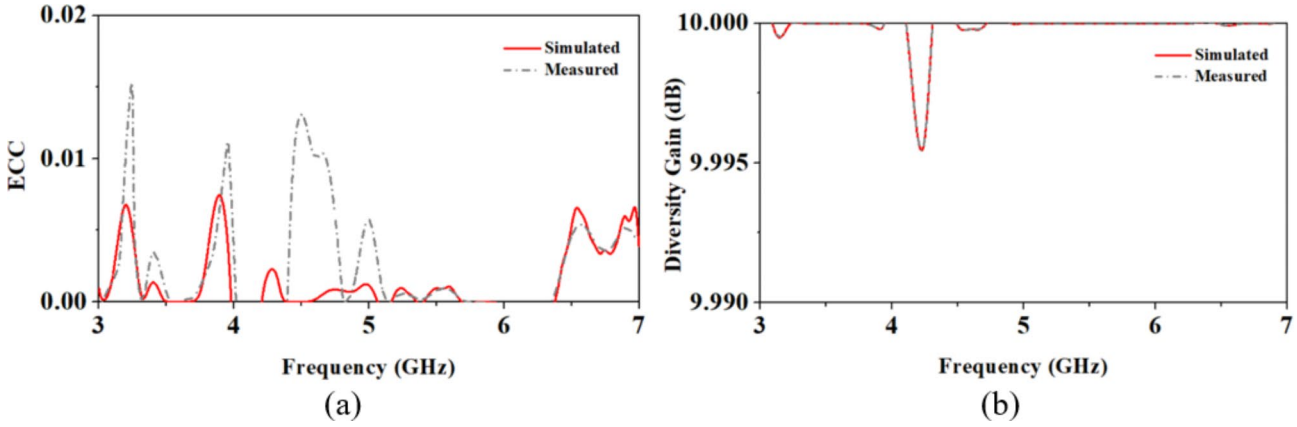

Fig. 30. Comparison of simulated and measured (**a**) ECC and (**b**) DG.

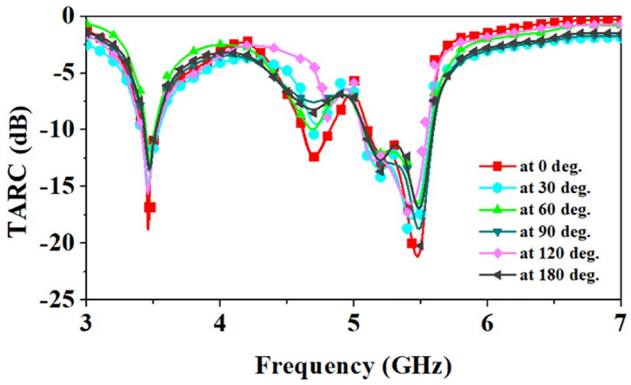

Fig. 31. Total active reflection coefficient (TARC) of proposed MIMO antenna at different phases of input signal.

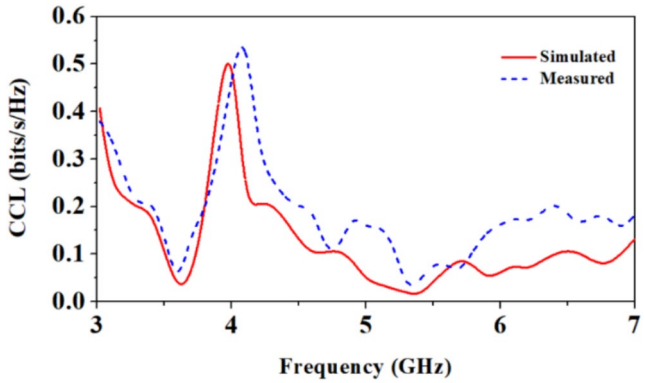

Fig. 32. Channel capacity loss (CCL) of the proposed MIMO antenna.

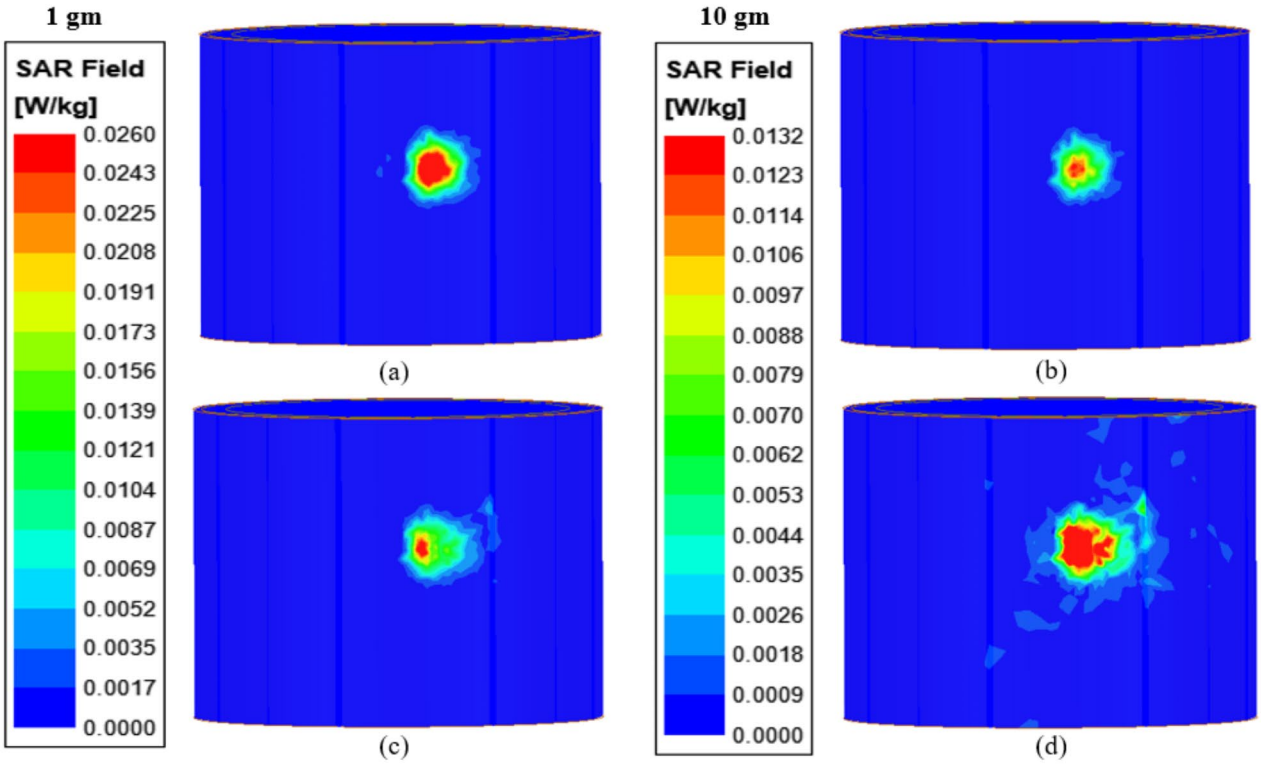

Fig. 33. Average SAR distribution in the phantom: (**a**) 1 g at 3.5 GHz, (**b**) 10 g at 3.5 GHz, (**c**) 1 g at 5.2 GHz, (**d**) 10 g at 5.2 GHz.

	Average SAR (on chest phantom)	
Frequency (GHz)	1 g	10 g
3.5	0.034	0.057
5.2	0.026	0.013

Table 4. Maximum average SAR values (1/10 gm) at 0.5 W of input power.

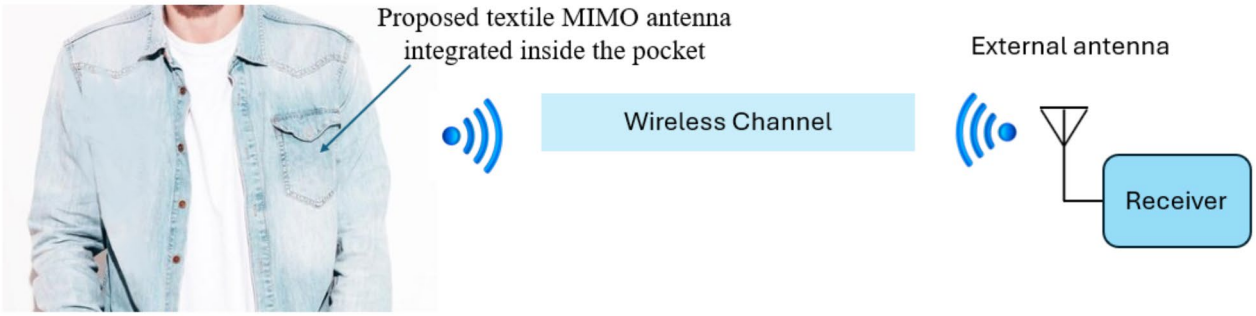

Fig. 34. Link budget calculation in hidden communication: Between wearable textile antenna integrated inside the pocket and the external antenna.

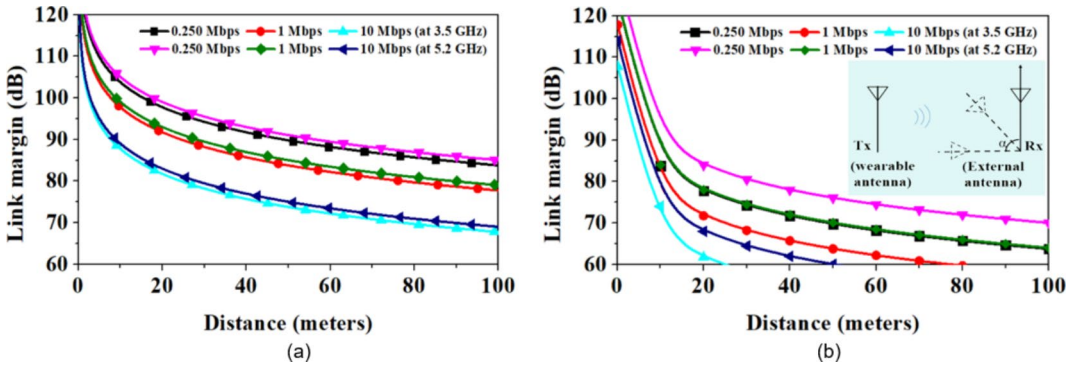

Fig. 35. Link margin for hidden communication of the proposed wearable textile MIMO antenna to the external antenna (**a**) when polarization losses are not considered (**b**) when polarization losses are considered (at $\alpha = 90^0$).

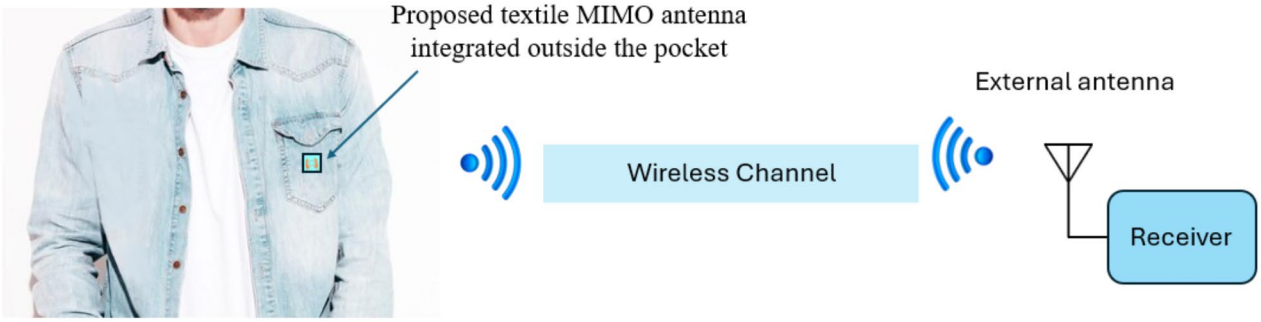

Fig. 36. Link budget calculation in the visible communication: Between wearable textile antenna integrated outside the pocket and external antenna.

to send biological signals from the textile MIMO antenna to an external antenna. The Friis transmission equation determines the link margin, as explained in[34]. The link margin versus the transmitter-receiver (T_x–R_x) distance graph is plotted (given in Figs. 35 and 37) using equations of the link margin[35].

Figure 34 shows the setup for the hidden communication (the MIMO antenna is inside the pocket). Here, the MIMO antenna's peak gain at 3.5 GHz and 5.2 GHz is 8.3 and 13.0 dBi, respectively. The link margin for this setup is shown in Fig. 35a; at 3.5 GHz, the maximum and minimum values of the link margin are 85.0 dB at 5.2 GHz and 67.7 dB at 3.5 GHz, respectively, at 100 m. Figure 35b shows the link margin when the external antenna is at non-line-of-sight 90^0. This condition considers polarization mismatch losses and causes reduced communication distance, as shown in (Fig. 35b). In this state, at 3.5 GHz, polarization mismatch losses are more than 5.2 GHz, as shown in Table 5; due to this, for a 10 Mbps data rate, at 3.5 GHz, up to 26 m communication

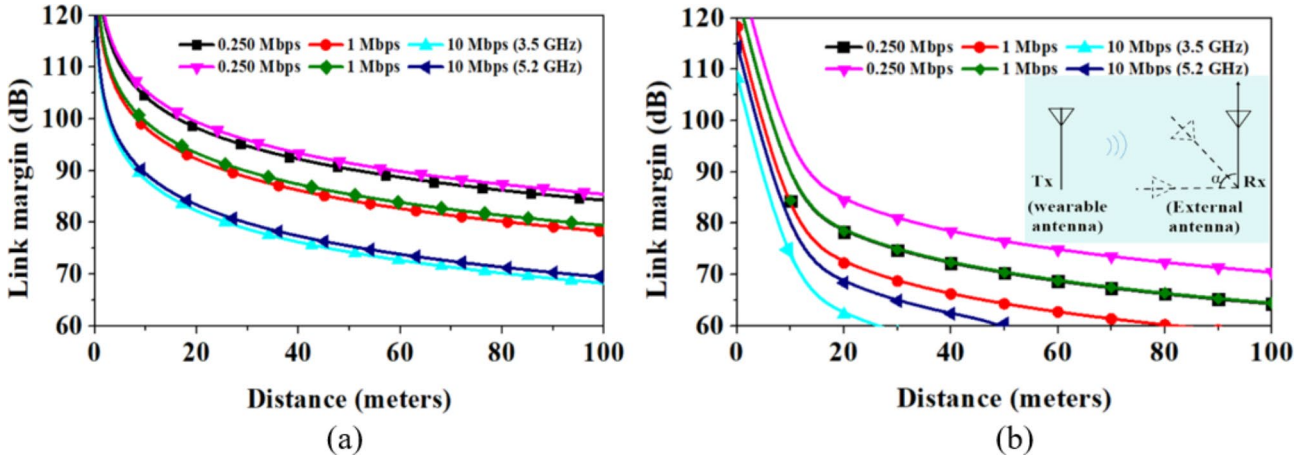

Fig. 37. Link margin for visible communication of the proposed wearable textile MIMO antenna to the external antenna (**a**) when polarization losses are not considered. (**b**) when polarization losses are considered (at $\alpha = 90^0$).

Transmitter			
	Frequency (GHz)		3.5/5.2
G_{t1}	Antenna gain (dBi) (Hidden)		8.3/13.0
G_{t2}	Antenna gain (dBi) (Visible)		8.8/13.4
P_t	Transmitter power (dBm)		16
	EIRP (dBm)		24.3/29.0
	EIRP (dBm)		24.8/29.4
Receiver			
G_r	Receiver antenna gain (dBi)		5
T_o	Ambient temperature (K)		293
	Boltzmann constant		1.38E−23
N_o	Noise power density (dB/Hz)		−203.9
v	Linear Axial Ratio		11.4/5.4
$e_{p\ (dB)}$	Polarization loss	$\alpha = 0^\circ / 90^\circ$	0.04/ 20
			0.15/14.68
Signal quality			
B_r	Bit rate (Mbps)		0.250, 1, 10
E_b/N_o	Ideal PSK (dB)		9.6
G_c	Coding gain (dB)		0
G_d	Fixing deterioration (dB)		2.5

Table 5. Link budget parameters for hidden and visible communication.

distance is possible for 60 dB link margin. The polarization mismatch losses are calculated from the equation given[36].

Figure 36 shows the setup for visible communication (when the MIMO antenna is attached outside the pocket). Here, the peak gain of the antenna at 3.5 and 5.2 GHz is 8.8 dBi and 13.4 dBi, respectively. The link margin for this setup is illustrated in Fig. 36; at 3.5 GHz, the maximum and minimum values of the link margin are 85.4 dB at 5.2 GHz and 68.2 dB at 3.5 GHz, respectively, at 100 m, as shown in (Fig. 37a). Figure 37b depicts the non-line-of-sight communication between the wearable and external antennas.

The graphs of Figs. 35 and 37 demonstrate that this wearable MIMO antenna can successfully communicate easily 100 m and 26 m and withstand additional path losses of more than 67 and 60 dB, respectively. In both cases (hidden and visible), the proposed wearable MIMO antenna's communication capability is almost the same, making it suitable for both communications.

Conclusion

A compact, textile MIMO antenna is proposed in the 5G sub-6 3.5 GHz and Wi-Fi 5.2 GHz bands. Due to its ultra-compact size, it integrates inside and outside the shirt's pocket and supports hidden and visible communication

with the external antenna. This MIMO antenna has a comparatively high gain of 8.3 and 13.0 dBi at 3.5 GHz and 5.2 GHz, respectively. Owing to the MIMO configuration and high gain, it can communicate more than 100 m of distance. We have also tested this MIMO antenna on different bending radii (both horizontally and vertically) and found it works efficiently. The proposed MIMO antenna exhibits low ECC values due to high channel isolation between the modified elliptical patch of the MIMO antenna. When equally fed at both ports, the SAR values of the proposed MIMO antenna are way below the standard values, which makes this antenna harmless for wearable applications. Therefore, the proposed compact wearable MIMO antenna with sufficient impedance bandwidths, decent gain, low ECC, good TARC, acceptable CCL values, and SAR values is suitable for 5G sub-6 3.5 GHz and Wi-Fi 5.2 GHz hidden and visible communications.

Data availability

All data generated or analysed during this study are included in this published article.

Received: 9 November 2024; Accepted: 13 January 2025
Published online: 11 February 2025

References

1. Sharma, D. & Kumar, S. Metamaterial based wearable and implantable antennas. in *Handbook of Nano-Metamaterials. Metamaterials Science and Technology* (ed. Choudhury, B., Tewary, V.K., Kanth, V. K.) 1–43, https://doi.org/10.1007/978-981-13-0261-9_50-1 (Springer, 2024).
2. Ejaz, A. et al. A high performance all-textile wearable antenna for wristband application. *Micromachines* **14**, 1–15 (2023).
3. Friedlander, B. Using MIMO to increase the range of wireless systems. In *Conference Record of the Thirty-Ninth Asilomar Conference onSignals, Systems and Computers*, 1404–1408 (IEEE, 2006).
4. West, D. M. Internet of things how 5G technology enables the health internet of things. *Cyber Resil. Syst. Netw.* https://doi.org/10.1007/978-3-319-77492-3_16 (2009).
5. Li, H., Sun, S., Wang, B. & Wu, F. Design of compact single-layer textile MIMO antenna for wearable applications. *IEEE Trans. Antennas Propag.* **66**, 3136–3141 (2018).
6. Mashagba, H. A. et al. A hybrid mutual coupling reduction technique in a dual-band MIMO textile antenna for WBAN and 5G applications. *IEEE Access* **9**, 150768–150780 (2021).
7. Jayant, S., Srivastava, G. & Kumar, S. Quad-port UWB MIMO footwear antenna for wearable applications. *IEEE Trans. Antennas Propag.* **70**, 7905–7913 (2022).
8. Saeidi, T., Al-Gburi, A. J. A. & Karamzadeh, S. A Miniaturized full-ground dual-band MIMO spiral button wearable antenna for 5G and sub-6 GHz communications. *Sensors* 23, (2023).
9. Wu, R., Dong, J. & Wang, M. Wearable polarization conversion metasurface MIMO antenna for biomedical applications in 5 GHz WBAN. *Biosensors* 13, (2023).
10. Gao, G. P. et al. A Compact dual-mode pattern-reconfigurable wearable antenna for the 2.4-GHz WBAN application. *IEEE Trans. Antennas Propag.* **71**, 1901–1906 (2023).
11. Jhunjhunwala, V. K. et al. A four port flexible UWB MIMO antenna with enhanced isolation for wearable applications. *Res. Eng.* **24**, (2024).
12. Pradeep, P., Basha, M. M., Gundala, S. & Syed, J. Development of wearable textile MIMO antenna for sub-6 GHz band new radio 5G applications. *Micromachines* **15**, (2024).
13. Khan, R. et al. Enhancing gain and isolation of a quad-element MIMO antenna array design for 5G sub-6 GHz applications assisted with characteristic mode analysis. *Sci. Rep.* **14**, 1–22. https://doi.org/10.1038/s41598-024-61789-7 (2024).
14. Technology, W., Composition, I. & Company, F. License Certificate. https://www.freepik.com/free-vector/wearable-technology-isometric-composition_%0A6414033.htm **4994** (2023).
15. Sharma, D., Kumar, S., Tiwari, R. N., Choi, H. C. & Kim, K. W. On body and off body communication using a compact wideband and high gain wearable textile antenna. *Sci. Rep.* **14**, 1–17. https://doi.org/10.1038/s41598-024-64932-6 (2024).
16. Sharma, D., Tiwari, R. N., Kumar, S., Sharma, S. & Matekovits, L. A Compact wearable textile antenna for NB-IoT and ISM band patient tracking applications. *Sensors* **24**, 5077 (2024).
17. Singh, R. K. et al. Compact and wearable yagi-like textile antennas for near-field UHF-RFID readers. *IEEE Trans. Antennas Propag.* **69**, 1324–1333 (2021).
18. Casula, G. A., Montisci, G. & Muntoni, G. A Novel design for dual-band wearable textile eighth-mode SIW antennas. *IEEE Access* **11**, 11555–11569 (2023).
19. Tiwari, R. N. et al. A low-profile dual-band millimeter wave patch antenna for high-speed wearable and biomedical applications. *Res. Eng.* **24**, 103212. https://doi.org/10.1016/j.rineng.2024.103212 (2024).
20. Das, R. & Yoo, H. A Multiband antenna associating wireless monitoring and nonleaky wireless power transfer system for biomedical implants. *IEEE Trans. Microwave Theory Tech.* **65**, 2485–2495 (2017).
21. Salonen, P., Rahmat-Samii, Y., Hurme, H. & Kivikoski, M. Effect of conductive material on wearable antenna performance: a case study of WLAN antennas. *IEEE Antennas Propag. Soc. AP-S Int. Symp. (Digest.)* **1**, 455–458 (2004).
22. Test & Tissue Properties *. *The journal of bone and joint surgery* https://itis.swiss/virtual-population/tissue-properties/database/dielectric-properties 58-A, 82–86 (1976).
23. Lan, I-C. S.-Y. C. and P. H. Pattern smoothness and gain enhancement of finite ground slot dipole antenna fed by conductor-backed coplanar waveguide. In *IEEE Antennas and Propagation Society International Symposium*, 1–4 (2008).
24. Mark, R., Rajak, N., Mandal, K. & Das, S. Semi elliptical two port MIMO antennas for wideband wireless application. *IEEE MTT-S International Microwave and RF Conference, IMaRC 2018* 1, 1–4 (2018).
25. Zulkifli, F. Y., Wahdiyat, A. I., Zufar, A., Nurhayati, N. & Setijadi, E. Super-wideband monopole printed antenna with half-elliptical-shaped patch. *Telecom* **5**, 760–773 (2024).
26. Boccia, L. & Amendola, G. Di Massa, G. A shorted elliptical patch antenna for GPS applications. *IEEE Antennas. Wirel. Propag. Lett.* **2**, 6–8 (2003).
27. Bahadori, K. & Rahmat-Samii, Y. A miniaturized elliptic-card UWB antenna with WLAN band rejection for wireless communications. *IEEE Trans. Antennas Propag.* **55**, 3326–3332 (2007).
28. Tu, Z. et al. A wideband cavity-backed elliptical printed dipole. *IEEE Antennas. Wirel. Propag. Lett.* **12**, 1610–1613 (2014).
29. Catarinucci, L., Colella, R. & Tarricone, L. Smart prototyping techniques for UHF RFID tags: electromagnetic characterization and comparison with traditional approaches. *Progress Electromagnet. Res.* **132**, 91–111 (2012).
30. Marriam, I., Tebyetekerwa, M., Chathuranga, H., Yang, S. & Yan, C. Fabrication techniques for wearable antennas. In *European microwave Conference 1747–1750CRC Press*. https://doi.org/10.23919/EuMC.2013.6687015 (2013).

31. Sharma, D., Tiwari, R. N., Kanaujia, B. K., Kumar, S. & Rambabu, K. Dual-band MIMO antenna data telemetry for dual-chamber leadless cardiac pacing on internet of things environment. *IEEE Internet Things J.* **11**, 9072–9085 (2024).
32. Sharma, D., Kanaujia, B. K. & Kumar, S. Compact multi-standard planar MIMO antenna for IoT/WLAN/Sub-6 GHz/X-band applications. *Wireless Netw.* **27**, 2671–2689. https://doi.org/10.1007/s11276-021-02612-3 (2021).
33. Gljušćić, P., Zelenika, S., Blažević, D. & Kamenar, E. Kinetic energy harvesting for wearable medical sensors. *Sens. (Switzerland)* **19**, (2019).
34. Rajagopalan, H. & Rahmat-Samii, Y. Wireless medical telemetry characterization for ingestible capsule antenna designs. *IEEE Antennas. Wirel. Propag. Lett.* **11**, 1679–1682 (2012).
35. Sharma, D. et al. Design and implementation of compact dual-band conformal antenna for leadless cardiac pacemaker system. *Sci. Rep.* **12**, 1–17. https://doi.org/10.1038/s41598-022-06904-2 (2022).
36. Yang, Y. et al. A 5.8 GHz circularly polarized rectenna with harmonic suppression and rectenna array for wireless power transfer. *IEEE Antennas. Wirel. Propag. Lett.* **17**, 1276–1280 (2018).

Author contributions

D.S. conceived and performed simulations and experiments and drafted the manuscript. D.S., R.N.T. and D.K.S conducted the experiment. D.S., R.N.T. and L.M. analyzed the results. L.M. supervised the overall work and provided funding for the experiments. All authors reviewed the manuscript.

Declarations

Competing interests

The authors declare no competing interests.

Additional information

Correspondence and requests for materials should be addressed to L.M.

Reprints and permissions information is available at www.nature.com/reprints.

Publisher's note Springer Nature remains neutral with regard to jurisdictional claims in published maps and institutional affiliations.